This is a preprint, the final version is subject to change, of the American Mineralogist (MSA)
Cite as Authors (Year) Title. American Mineralogist, in press.
(DOI will not work until issue is live.) DOI: http://dx.doi.org/10.2138/am.2014.4593

REVISED VERSION 1

(#4593R)

CORRECTION (July 16th, 2013)

Perbøeite-(Ce) and alnaperbøeite-(Ce), two new members of the epidote - törnebohmite polysomatic series: chemistry, structure, dehydrogenation and clue for a sodian epidote end-member

PAOLA BONAZZI,[1,*] GIOVANNI O. LEPORE,[1] LUCA BINDI,[1] CHRISTIAN CHOPIN,[2]
TOMAS A. HUSDAL[3] and OLAF MEDENBACH[4]

[1]Dipartimento di Scienze della Terra, Università di Firenze, Via La Pira 4, I-50121 Florence, Italy
[2]Laboratoire de Géologie, Ecole normale supérieure - CNRS, 24 rue Lhomond, F-75005 Paris, France
[3]Veslefrikk 4, N-8028 Bodø, Norway
[4]Institut für Geologie, Mineralogie und Geophysik, Ruhr-Universität Bochum, D-44780 Bochum, Germany

ABSTRACT

In yttrian fluorite from pegmatites of the Tysfjord granite, Norway, grayish green to very pale green gatelite-like crystals occur along with millimeter-size aggregates of Y-silicates as a late primary phase; they are associated with allanite-(Ce), bastnäsite-(Ce) and intimately inter- or overgrown by törnebohmite-(Ce). Sub- to euhedral crystals, up to 400 μm in size, are chemically zoned between two near-end-member compositions that imply the existence of two new members of the polysomatic gatelite group – in which *ET* polysomes are composed of *E* modules with epidote-type structure alternating with *T* modules of

25 törnebohmite-type structure. The two new minerals form a continuous solid-solution series,
26 along which two crystals of intermediate compositions served for species definition. Their
27 electron-microprobe analyses yield the empirical formulae
28 $(Ca_{1.00}Mn_{0.03}Na_{0.08}La_{0.51}Ce_{1.30}Pr_{0.16}Nd_{0.62}Sm_{0.10}Gd_{0.06}Dy_{0.03}Er_{0.01}Y_{0.06}Th_{0.01})_{\Sigma 3.97}$
29 $(Al_{3.21}Fe^{2+}_{0.79})_{\Sigma 4.00}Si_{5.01}O_{20}(OH)_2$ for perbøeite-(Ce) [IMA 2011-55] and
30 $(Ca_{1.10}Mn_{0.03}Na_{0.20}La_{0.42}Ce_{1.14}Pr_{0.16}Nd_{0.60}Sm_{0.13}Gd_{0.07}Dy_{0.03}Er_{0.01}Yb_{0.01}Y_{0.12}Th_{0.02})_{\Sigma 4.04}$
31 $(Al_{3.54}Fe^{2+}_{0.40}Mg_{0.02})_{\Sigma 3.96}Si_{4.99}O_{20}(OH)_2$ for alnaperbøeite-(Ce) [IMA 2012-54]. The respective
32 end-member formulae are $^{A}(Ce_3Ca)^{M}(Al_3Fe^{2+})Si_2O_7(SiO_4)_3O(OH)_2$, which requires Ce_2O_3
33 45.10, CaO 5.14, FeO 6.58, Al_2O_3 14.01, SiO_2 27.52, H_2O 1.65, total 100.00 wt%; and
34 $^{A}(Ce_{2.5}CaNa_{0.5})^{M}(Al_4)Si_2O_7(SiO_4)_3O(OH)_2$, which requires Ce_2O_3 40.86, CaO 5.58, Na_2O 1.54,
35 Al_2O_3 20.31, SiO_2 29.92, H_2O 1.79, total 100.00 wt%. Cell parameters of perbøeite-(Ce) and
36 alnaperbøeite-(Ce) for these crystals are *a* 8.9277(6) and 8.9110(4), *b* 5.6548(6) and
37 5.6866(2), *c* 17.587(1) and 17.5252(7) Å, β 116.475(8) and 116.300(5)°, *V* 794.8(1) and
38 796.13(7) $Å^3$, respectively. Members of the perbøeite-(Ce)–alnaperbøeite-(Ce) solid solution
39 are topologically identical to the minerals gatelite-(Ce) and västmanlandite-(Ce). Structural
40 data (space group $P2_1/m$) were obtained for the holotype crystals and for a number of crystals
41 with intermediate composition. Structural refinements of a crystal annealed step-wise in air
42 confirm that most of Fe in M3 is divalent before heating and show that
43 oxidation/dehydrogenation takes place mostly in the *E* module (M3 and H1). Perbøeite-(Ce)
44 derives from gatelite-(Ce) by the homovalent substitution [$^{M3}Fe^{2+} \rightarrow {}^{M3}Mg$]. Alnaperbøeite-
45 (Ce) derives from perbøeite-(Ce) or gatelite-(Ce) by the coupled heterovalent substitutions
46 [$^{A}Na^{+} + {}^{M3}2Al^{3+} \rightarrow {}^{A}REE + {}^{M3}2(Fe^{2+}$ or Mg)].

47 Törnebohmite-(Ce) associated with alnaperbøeite-(Ce) is Na-free whereas coexisting
48 allanite is Na-bearing and shows the same coupled substitution between A and M sites as the
49 one relating perbøeite-(Ce) and alnaperbøeite-(Ce) ($Na_{0.5}Al \leftrightarrow REE_{0.5}Fe^{2+}$). This could

This is a preprint, the final version is subject to change, of the American Mineralogist (MSA)
Cite as Authors (Year) Title. American Mineralogist, in press.
(DOI will not work until issue is live.) DOI: http://dx.doi.org/10.2138/am.2014.4593

suggest, although crystallographic evidence is inconclusive, that Na incorporation in the *ET* polysome occurs in the *E* module alone (A2 or A1 sites), leading to the sodian *E* end-member $^{A}(CaREE_{0.5}Na_{0.5})^{M}(Al_3)Si_2O_7(SiO_4)O(OH)$. In any event, this new epidote end-member is needed to account for up to ca. 10 mol. % of the composition of allanite-group minerals, in which Na_2O contents may reach 0.3 wt%. Sodium has to be sought in epidote-supergroup and gatelite-group minerals.

Keywords: new mineral, perbøeite-(Ce), alnaperbøeite-(Ce), Tysfjord granite (Norway), polysomatic series, epidote supergroup, crystal structure, chemical composition.

INTRODUCTION

Minerals belonging to the gatelite group, i.e. gatelite-(Ce) (Bonazzi et al. 2003) and västmanlandite-(Ce) (Holtstam et al. 2005), can be regarded as iso-topological *ET* type polysomes within a polysomatic series having epidote and törnebohmite as end-members. Their structure (Figure 1) is a regular alternating stacking of (001) slabs of epidote-type structure (*E*) and ($\bar{1}02$) slabs of törnebohmite-type structure (*T*) (Shen and Moore 1982). The *T* modules in both minerals have the same composition as the mineral törnebohmite, $(Ce,La)_2Al[SiO_4]_2(OH)$, whereas the chemical variability of the *E* module characterizes the mineral, even if all the *E* modules known so far belong to the allanite group. Specifically, the *E* module is of dissakisite-(Ce) composition, $CaCeAl_2MgSi_2O_7(SiO_4)O(OH)$ (Grew et al. 1991; Rouse and Peacor 1993) in gatelite-(Ce) and of dollaseite-(Ce) composition, $CaCeAlMg_2Si_2O_7(SiO_4)F(OH)$ (Peacor and Dunn 1988) in västmanlandite-(Ce). Moreover, the gatelite-like minerals from the Bergslagen mining region of south-central Sweden characterized by Holtstam and Andersson (2007) can be essentially described as members of the solid-solution between västmanlandite-(Ce) and an unnamed mineral having the *E* module

This is a preprint, the final version is subject to change, of the American Mineralogist (MSA)
Cite as Authors (Year) Title. American Mineralogist, in press.
(DOI will not work until issue is live.) DOI: http://dx.doi.org/10.2138/am.2014.4593

of ferriallanite-(Ce) composition, $CaCeFe^{3+}AlFe^{2+}Si_2O_7(SiO_4)O(OH)$ (Kartashov et al. 2002; Kolitsch et al. 2012).

The recent finding of two new *ET* type polysomes extending the range of known compositions led to the definition of two new species, perbøeite-(Ce) and alnaperbøeite-(Ce), approved by the Commission on New Minerals, Nomenclature and Classification, IMA (2011-055 and 2012-054, respectively). Their definition is based on the analytical evidence of a continuous solid solution between two near-end-member compositions of new *ET* polysomes, and on the structure refinement of crystals of intermediate compositions, by lack of homogeneous crystals of near-end-member composition. In addition, the analysis of the structural variations observed on a crystal heated in air offers the opportunity to explore possible differences in response to the induced oxidation-dehydrogenation reaction within *E* and *T* modules.

Holotype material is deposited in the collections of the Museo di Storia Naturale, Sezione di Mineralogia e Litologia, Università di Firenze, Via La Pira 4, I-50121, Firenze, Italy, under catalogue number 3110/I [perbøeite-(Ce)] and 3114/I [alnaperbøeite-(Ce)].

GEOLOGICAL SETTING, OCCURRENCE AND PARAGENESIS

Hundholmen, Stetind and Nedre Eivollen pegmatites belong to a series of quartz-microcline pegmatites of the niobium-yttrium-fluorine family found in the Tysfjord granite (Norway), a ca. 1742 ± 46 Ma old granitic gneiss deformed during the Caledonian orogeny (Andresen and Tull 1986). Main accessory minerals in these pegmatites include allanite-(Ce), fergusonite-(Y), columbite-(Fe), beryl, various sulfides (pyrite, pyrrhotite, arsenopyrite) and fluorite, particularly an yttrium-rich variety, yttrian fluorite, with abundant inclusions of various REE-minerals (Husdal 2008). The new species hundholmenite-(Y) (Raade et al. 2007), stetindite (Schlüter et al. 2009), fluorbritholite-(Y) (Pekov et al. 2011), atelisite-(Y)

(Malcherek et al. 2012), bastnäsite-(Nd) (IMA 2011-062), cayalsite-(Y) (IMA 2011-094) and schlüterite-(Y) (IMA 2012-015) were found in yttrian fluorite masses.

Both perbøeite-(Ce) and alnaperbøeite-(Ce) occur as isolated or loosely aggregated, sub- to euhedral crystals, up to 400 μm in size within white yttrian fluorite. Crystals have a stout prismatic morphology elongated along [010]. Perbøeite-(Ce) and alnaperbøeite-(Ce) appear very similar to each other: they are transparent with vitreous lustre and their color ranges from pale greyish green [perbøeite-(Ce)] to very pale green [alnaperbøeite-(Ce)].

At Hundholmen [type-locality for perbøeite-(Ce)] and Stetind [type-locality for alnaperbøeite-(Ce)] these minerals [and törnebohmite-(Ce)] occur both as inclusions in the fluorite groundmass and, along with some isolated crystals of allanite-(Ce) and bastnäsite-(Ce), within millimeter-size aggregates of one or several Y-silicates [fluorthalénite-(Y)/thalénite-(Y), kuliokite-(Y), hundholmenite-(Y)], also included in yttrian fluorite (Fig. S1 in Supplementary Materials). In the Hundholmen material pyrite was also observed as accessory mineral; in the Stetind material, vyuntspakhkite-(Y) and thorite with zircon inclusions. Material from Nedre Eivollen shows a somewhat different texture, in which subhedral perbøeite-(Ce)/alnaperbøeite-(Ce) associated with thalénite-(Y)/fluorthalénite-(Y) [and minor allanite-(Ce), törnebohmite-(Ce), bastnäsite-(Ce) and fluorbritholite-(Y)] fill or line millimeter-size interstices and voids in the fluorite groundmass [with bastnäsite-(Ce) and fluocerite-(Ce) inclusions], the remaining void spaces being ultimately filled by massive albite. Perbøeite-(Ce)/alnaperbøeite-(Ce) therefore appear as late primary minerals in the pegmatite evolution. They are relatively abundant in the material studied, whereas allanite-(Ce), although commonly reported there, is subordinate.

At the three localities, both new minerals are consistently intergrown with and/or overgrown by lamellae of törnebohmite-(Ce), or exhibit minute irregular intergrowths with törnebohmite-(Ce) (Fig. 2). As also revealed by high-contrast back-scattered electron imaging

This is a preprint, the final version is subject to change, of the American Mineralogist (MSA)
Cite as Authors (Year) Title. American Mineralogist, in press.
(DOI will not work until issue is live.) DOI: http://dx.doi.org/10.2138/am.2014.4593

of polished sections, especially in the Stetind material, crystals are more or less concentrically zoned, with lower-mass cores and higher-mass rims, overgrowths and fillings of cracks or of dissolution embayments in the crystal (Fig. S2 and S3 in Supplementary Materials).

EXPERIMENTAL METHODS

X-ray data collection

Several single crystals were mounted on a CCD-equipped Oxford Diffraction Excalibur 3 diffractometer. The unit-cell dimensions of twelve examined crystals are in the range a = 8.90-8.95, b = 5.65-5.69, c = 17.50-17.65 Å, β = 116.2-116.7° (Table 1), without any evidence of doubling of the translation unit along the **a**-axis. Although the crystals were examined with long exposure times, neither superstructure reflections such as in gatelite-(Ce) nor the weak, continuous streaking as in västmanlandite-(Ce) were detected. One crystal (ST2_02) was annealed for 48 h at selected temperatures ranging from 350 to 750 °C in a Carbolite CWF1200 furnace allowing the crystal to cool slowly in the furnace down to room temperature. Intensity data for natural and heat-treated crystals were collected with an Oxford Diffraction Xcalibur 3 diffractometer with a monochromatized Mo$K\alpha$ X-radiation, equipped with a Sapphire 2 CCD detector (see Table 1 for details). Intensity integration and standard Lorentz-polarization correction were performed with the *CrysAlis* RED (Oxford Diffraction 2006) software package. The program ABSPACK in *CrysAlis* RED (Oxford Diffraction 2006) was used for the absorption correction.

Structure refinement

Given the absence of superstructure *hkl* reflections with $h = 2n + 1$, like in the case of västmanlandite-(Ce) the structure was refined in the $P2_1/m$ space group, instead of $P2_1/a$ like in gatelite-(Ce). The atomic parameters of gatelite-(Ce) (transformed in the $P2_1/m$ setting)

were used as starting model. The full-matrix least-squares program SHELXL-97 (Sheldrick 2008) was used for the refinement of the structure. One oxygen atom (O15) was found to be located out of the mirror plane (O15-O15 in the range 0.72 - 0.80 Å) and partially occupied (50%). In most cases three-dimensional difference Fourier synthesis yielded the position of two H atoms, close to O11 (H1) and O10 (H2). Nonetheless, in most of the investigated crystals the diffraction quality allowed the refinement of the atomic parameters of H1 alone.

The site population of all the metal positions was allowed to vary using different couples of scattering factors for ionized species as follows: Ca^{2+} vs. Ce^{3+} (A sites), Al^{3+} vs. Fe^{3+} (M1 and M2), Al^{3+} vs. Fe^{2+} (M3). Both scattering curves and $\Delta f'$, $\Delta f''$ coefficients were taken from the *International Tables for X-ray Crystallography*, volume C (Wilson and Prince 1999). Details of the anisotropic refinements are summarized in Table 1.

In analogy with the epidote-supergroup[1] members, M3 is the key-site to discriminate a new mineral species (Armbruster et al. 2006) in gatelite-like minerals. Two of the studied crystals, one showing aluminum dominance (ST4_11, M3 = $Al_{0.60}Fe_{0.40}$) and one iron dominance (HU_02, M3 = $Fe_{0.60}Al_{0.40}$), were thus selected to characterize the two new mineral species alnaperbøeite-(Ce) and perbøeite-(Ce).

Fractional atomic coordinates and equivalent isotropic-displacement parameters of ST4_11 and HU_02 are reported in Table 2. Table 3[2] reports the atom coordinates and the ADPs of the other studied crystals. Table 4[2] lists the observed and calculated structure factors for all the investigated crystals.

The X-ray powder diffraction pattern was collected with an automated Philips PV110 diffractometer using Ni-filtered Cu$K\alpha$ radiation by selecting greyish green crystals from sample ST2 in which perbøeite-(Ce) prevails on alnaperbøeite-(Ce). However, the unit cell

[1] According to the recent standardization of mineral group hierarchies (Mills et al. 2009), the terms 'group' and 'subgroup' used by Armbruster et al. (2006) for the epidote nomenclature have been changed to 'supergroup' and 'group', respectively.

[2]Tables 3 and 4 are deposited...

obtained by least-squares refinement of 25 measured reflections [a = 8.9120(7), b = 5.6691(3), c = 17.473(1) Å, β = 116.147(6)°, V = 792.45(8) Å^3] and a comparison with calculated X-ray powder patterns (Table 5) reveals a likely admixture with Al-rich grains.

Chemical analyses

The two holotype crystals and the crystal ST2_02 were embedded in epoxy and polished for electron microprobe analysis (EMPA). Additional EMPA data for alnaperbøeite-(Ce) and perbøeite-(Ce) solid solution and coexisting minerals were obtained on polished rock samples from Stetind (ST2 and ST4) and Nedre Eivollen (NE) and on a minute fragment from Hundholmen. Analyses were performed using Cameca SX100 and SXFive electron microprobes at Centre Camparis, Paris, in wavelength-dispersive mode at 15 kV, 15 nA beam current, 2 μm beam diameter, 5 to 30 s counting time on both peak and background, using the following standards: apatite (F and P *K*α), albite (Na*K*α), diopside (Mg, Si and Ca *K*α), orthoclase (Al and K *K*α), $MnTiO_3$ (Ti and Mn *K*α), hematite (Fe*K*α), $SrSiO_3$ (Sr*L*α), $BaSO_4$ (Ba*L*α), monazite (Ce*L*α, Th*M*α), La_3ReO_8 (La*L*α), NdCu (Nd*L*β), Sm_3ReO_8 (Sm*L*β) and REE-bearing glasses (Pr, Gd, Dy, Ho and Er *L*β, Yb and Y *L*α), with due consideration of possible interferences and φρ*Z* data reduction (PAP, Pouchou and Pichoir, 1984). Table 6 reports chemical analyses and atomic ratios for the three single crystals investigated. Chemical analyses obtained along the solid-solution series on zoned crystals are listed in Table 7[3] whereas Table 8 reports the analyses of coexisting minerals in Stetind (ST) and Nedre Eivollen (NE). The relatively low analytical totals obtained for the REE-rich minerals may reflect the difficulty in analyzing accurately all the REEs.

PHYSICAL PROPERTIES

[3] Table 7 is deposited…

Both minerals are brittle, with a good {100} an imperfect {001} cleavage. Crystals are elongated along *b*, with the main forms {101}, {100} and {001}. They are transparent, biaxial, optically positive with pleochroism from absent in alnaperbøeite-(Ce) to very weak in perbøeite-(Ce) (Table 9). There is no evidence of metamictization. Density could not be measured due to the zoned nature of the crystals and to the presence of lamellae of törnebohmite-(Ce) within them. The calculated values of density, obtained using the empirical formulae of single crystals used for the structural study, and the mean refractive indices, calculated according to the Gladstone-Dale relationship (Mandarino 1976), are reported in Table 9.

MINERAL CHEMISTRY

Major elements in the *E*, *T* and *ET* phases

There is no P and Pb, virtually no F, Ti, Sr, Ba and U in the coexisting *E*, *T* and *ET* compounds. Mg is minor in allanite, even more so in perbøeite-(Ce), and absent in törnebohmite-(Ce), showing a partitioning similar to Fe among these phases. The situation is different for Mn, which is substantial only in some allanite-(Ce) crystals whereas it is minor to trace in gatelite-type phases and a trace in törnebohmite-(Ce). Its behavior is not related to that of Fe. The significant presence of Na is a major new feature, with Na_2O contents increasing up to 0.84 wt% from perbøeite-(Ce) to alnaperbøeite-(Ce), variable in allanite-(Ce) (up to 0.29 wt%), and as traces in törnebohmite-(Ce). Light REE are dominant over heavy ones in all four phases, but clearly less so in törnebohmite-(Ce), and marginally less in alnaperbøeite-(Ce) than in perbøeite-(Ce). Yttrium is present in the four phases, with average oxide contents of 0.3 wt% in allanite-(Ce), 2.2 wt% in törnebohmite-(Ce) and, in the *ET* phases, Y_2O_3 contents ranging between 0.3 and ca. 1.0 wt% in perbøeite-(Ce) and ca. 1.0 to 2.0 wt% in alnaperbøeite-(Ce), grossly correlated with Al and Na contents. Thorium is minor

to trace: very low in allanite-(Ce), variable (up to 0.5 wt% ThO_2) in törnebohmite-(Ce) and, although with much scatter, clearly increasing up to this value from perbøeite-(Ce) to alnaperbøeite-(Ce).

On the basis of crystallographic knowledge, structural formulae were first tentatively calculated on the same basis of nine tetrahedral + octahedral cations (Si+P+Al+Ti+Fe+Mg) for all the phases of the polysomatic series, i.e. allanite-(Ce), törnebohmite-(Ce) and perbøeite-(Ce)/alnaperbøeite-(Ce) (Table 7). The advantages are i) to spread the analytical uncertainty on several elements rather than tying it to Si alone, ii) there is no assumption on Fe and Mn valence states nor on the A-site occupancy, iii) if some REEs are not analyzed, the results for the other elements are unaffected. The only assumption made is that Mn and Y are assigned to the A sites.

This preliminary calculation showed that, for the simpler compound törnebohmite-(Ce), the mean and standard deviation values were Si = 5.99(2) and Al = 3.00(2) atoms per chosen formula unit (apfu) for all the analyses (n = 8). Likewise, for all perbøeite-(Ce)/alnaperbøeite-(Ce) analyses (n = 54), Si = 5.00(5) apfu and the sum of M and A cations [Σ(M+A)] was 7.96(8) apfu. This indicated the reliability of Si and Al analysis and that there is very little A vacancy, if any, in the new gatelite-type phases (see below). The case of allanite was more subtle, with a mean Si = 4.55(3) instead of the ideal 4.50 atoms for this calculation basis. Scrutiny of analyses showed that the Si excess was directly linked to high Mn values. Therefore, the assumption of all Mn in the A site does not hold for these allanites, and the allanite formulae were recalculated on a Si = 3 basis, yielding a mean [Σ(M+A)] = 4.98(3) apfu for all allanite analyses (n = 10), with on average one third of the total Mn content in octahedral position.

Considering that REEs are difficult to analyze and that some were not analyzed, the question arises as to whether the slight deficit in A+M cations is real. Indeed, such a deficit

increases from allanite-(Ce) (0.4%) to gatelite-type (0.5%) to törnebohmite-(Ce) (0.9%), i.e. as a function of the REE amounts in the mineral. The slightly low mean analytical totals [97.3, 95.9 and 95.3 wt% for allanite-(Ce), gatelite-type and törnebohmite-(Ce), respectively] may hint to the same conclusion, namely that the slight deficit of A+M cations reflects an analytical deficit in REE and is therefore essentially an *apparent* A-site deficit. This can also account for the low mean refractive indices calculated on the basis of the analyses, as compared to the measured one (Table 9).

On this firm ground, formulae were then calculated and are presented here on the basis of $O_{20}(OH)_2$ for gatelite-type phases, $O_{12}(OH)$ for allanite-(Ce) and $O_8(OH)$ for törnebohmite-(Ce), assuming divalent iron and manganese. The dominantly divalent state of iron is confirmed by crystallographic data and makes the presence of trivalent manganese unlikely.

Two new *ET* phases

The empirical formulae calculated from the EMP analyses of the three single crystals investigated (Table 6) are:

$(Ca_{1.10}Mn_{0.03}Na_{0.20}La_{0.42}Ce_{1.14}Pr_{0.16}Nd_{0.60}Sm_{0.13}Gd_{0.07}Dy_{0.03}Er_{0.01}Yb_{0.01}Y_{0.12}Th_{0.02})_{\Sigma 4.04}$
$(Al_{3.54}Fe^{2+}_{0.40}Mg_{0.02})_{\Sigma 3.96}Si_{4.99}O_{20}(OH)_2$ for ST4_11

$(Ca_{1.00}Mn_{0.03}Na_{0.08}La_{0.51}Ce_{1.30}Pr_{0.16}Nd_{0.62}Sm_{0.10}Gd_{0.06}Dy_{0.03}Er_{0.01}Y_{0.06}Th_{0.01})_{\Sigma 3.97}$
$(Al_{3.21}Fe^{2+}_{0.79})_{\Sigma 4.00}Si_{5.01}O_{20}(OH)_2$ for HU_02, and

$(Ca_{1.01}Mn_{0.03}Na_{0.09}La_{0.46}Ce_{1.25}Pr_{0.16}Nd_{0.75}Sm_{0.13}Gd_{0.05}Dy_{0.01}Ho_{0.01}Er_{0.02}Y_{0.07}Th_{0.01})_{\Sigma 4.05}$
$(Al_{3.13}Fe^{2+}_{0.79}Mg_{0.03})_{\Sigma 3.95}Si_{5.02}O_{20}(OH)_2$ for ST2_02 (before heating).

The total electron number ($e^-_A + e^-_M$) calculated on the basis of the chemical formulae derived from microprobe data (239.5, 251.0 and 254.3 for ST4_11, HU_02 and ST2_02, respectively) is in satisfactory accord with that obtained by the structure refinements (240.5, 253.6 and 252.2, respectively). In HU_2 and ST2_02, the M-sites cation content

($Al_{3.21}Fe^{2+}_{0.79}$ and $Al_{3.13}Fe^{2+}_{0.79}Mg_{0.03}$, respectively) suggests Fe-dominance in M3, as confirmed by the structure refinements, and, given the classical population of the A sites, point to an *E* module dominantly of allanite-(Ce) composition.

This composition is new among the *ET* polysomes (cf. Introduction) and is the basis for the definition of the new species perbøeite-(Ce). The end-member formula of perbøeite-(Ce) is therefore $^{A}(Ce_3Ca)^{M}(Al_3Fe^{2+})Si_2O_7(SiO_4)_3O(OH)_2$, which requires Ce_2O_3 45.10, CaO 5.14, Al_2O_3 14.01, FeO 6.58, SiO_2 27.52, H_2O 1.65, total 100.00 wt%.

The analysis of ST4_11 implies Al dominance in all M sites, M3 included, therefore pointing to a novel *ET* compound which, unlike all others, has a trivalent cation in M3. Charge balance is achieved in the A sites by substitution of trivalent REEs by divalent Ca to some extent but, essentially, by monovalent Na. The resulting composition is necessarily new among the *ET* phases and thus the basis for the definition of the new species alnaperbøeite-(Ce). The end-member formula of alnaperbøeite-(Ce) is $^{A}(Ce_{2.5}CaNa_{0.5})^{M}(Al_4)Si_2O_7(SiO_4)_3O(OH)_2$, which requires Ce_2O_3 40.86, CaO 5.58, Na_2O 1.54, Al_2O_3 20.31, SiO_2 29.92, H_2O 1.79, total 100.00 wt%.

Compositional variations: a solid-solution series

A first-order feature is the continuity of the chemical trends between near-end-member values as shown in Figure 3, where the calculated atomic contents are plotted as a function of the number of Al atoms pfu, which varies between 3 [as in end-member perbøeite-(Ce)] and 4 [as in end-member alnaperbøeite-(Ce)]. Typical crystal-core compositions are near 3.8–3.7 Al apfu in samples ST4 and NE and may grade within the same crystal to rim compositions of 3.2–3.1 Al, whereas they evolve from 3.4 (cores) to 3.0 Al (rims) in sample ST2. The continuity across the series is evidence for a continuous solid solution between the two new minerals, with a divide between the two species at the 50:50 boundary (i.e. 3.5 Al apfu) in the

296 case of a pure binary system. Figure 3 illustrates the main substitutions acting across the
297 series: with decreasing Al, a near 1/1 increase of Fe (substitution in M3), coupled to a clear
298 decrease of Na and increase of REEs (substitution in A sites) to reach an extreme composition
299 for Al = 3 that has nearly exact end-member perbøeite-(Ce) stoichiometry. For the more Al-
300 rich compositions the departure of Ca contents from unity (> 1) reveals that the analyzed solid
301 solution is not purely binary between the perbøeite-(Ce) and alnaperbøeite-(Ce) end-members,
302 but ternary with some contribution (about 10 mol%) of an *ET* polysome having clinozoisite as
303 *E* module.

304 The associated allanite crystals (Table 8a) reflect the compositional variations
305 observed in the *ET* phases between samples: they are more Al-, Ca- and Na-rich (up to 2.17
306 Al, 0.99 Ca and 0.05 Na apfu) and show no Fe^{3+} in sample NE where alnaperbøeitic crystal
307 cores are common; they are more Fe- (0 to 17% trivalent, 7% on average) and REE-rich and
308 Al-, Ca- and Na-poor in sample ST2 (from a locality where hematite occurs), in which *ET*
309 crystals have only perbøeitic compositions. Obviously, the same coupled substitutions relating
310 perbøeite-(Ce) and alnaperbøeite-(Ce) are also acting in coexisting allanite, to an extent
311 discussed below in more detail.

312 In contrast, associated törnebohmite-(Ce) appears, with a nearly constant Si/Al ratio
313 and at most 0.25 wt% CaO and 0.56 wt% ThO_2, as the least variable in composition among
314 the *E*, *T* and *ET* compounds, the only variations being among the REE (with up to 2.76 wt%
315 Y_2O_3).

316

317 ## DESCRIPTION OF THE STRUCTURE AND CATION DISTRIBUTION

318 Members of the perbøeite-(Ce)–alnaperbøeite-(Ce) solid solution are topologically
319 identical to the minerals gatelite-(Ce) and västmanlandite-(Ce). Their structure consists of
320 edge-sharing octahedral chains running along the **b** axis, cross-linked to each other by three

non-equivalent SiO_4 isolated tetrahedra and one Si_2O_7 group. The large cavities are occupied by REE, Ca and Na with Ca dominant at the A1 site and REE dominant at A2, A3 and A4 (Fig. 4). Three independent octahedral sites are present in the structure: M1 octahedra form branched chains with M3 octahedra alternately attached on opposite sides, whereas M2 octahedra form single chains. As in the case of gatelite-(Ce), the crystal-chemical details of the octahedral framework closely resemble those of the homologous sites in the structure of epidote-supergroup minerals, in particular in those belonging to the allanite group (Armbruster et al. 2006), and törnebohmite-(Ce) (Shen and Moore 1982), respectively. The M1 and M2 sites (<M1-O> = 1.924-1.930 Å and <M2-O> = 1.892-1.899 Å, Table 10) are occupied mainly by Al, whereas the cation population at the M3 octahedron, the largest and most distorted in the structure and the most suitable to incorporate divalent cations, differentiates perbøeite-(Ce) from alnaperbøeite-(Ce). In particular, in HU_02 perbøeite-(Ce) crystal the <M3-O> distance (2.107 Å) is consistent with the dominance of Fe^{2+} at this site, whereas Al prevails over Fe^{2+} in ST4_11 alnaperbøeite-(Ce) crystal (<M3-O> = 2.051 Å). Taking into account the refined site scattering (Table 10) and estimating the Fe^{3+} content on the basis of pure <M3-O> distances derived from known interatomic distances for members of the epidote supergroup ($<Al\text{-}O>_{M3}$ = 1.968 Å, $<Fe^{3+}\text{-}O>_{M3}$ = 2.055 Å, $<Fe^{2+}\text{-}O>_{M3}$ = 2.175 Å; Bonazzi and Menchetti 1995), a cation population can be estimated. In particular, M3 = 0.64 Fe^{2+} + 0.08 Fe^{3+} + 0.28 Al and M3 = 0.60 Al + 0.40 Fe^{2+} for HU_02 and ST4_11, respectively. This empirical method to estimate the M3 site population suggests the presence of Fe^{3+} not only in HU_02 crystal but also in most of the investigated crystals wherein Fe^{3+} ranges from 0.00 to 0.17 apfu (Table 10). Site-scattering refinement also indicates that small amounts of Fe substitute for Al in M1 and M2 sites (up to 0.05 apfu in both sites), which, in keeping with the crystal chemical requirements of the epidote-supergroup minerals, should be assumed as Fe^{3+}. When normalized on the basis of $\sum$(M+T) = 9 apfu, many of the chemical

346 analyses (Tables 6 and 7) would lead to sums of positive charges slightly higher than those
347 corresponding to $O_{20}(OH)_2$. Thus, the hypothesized presence of Fe^{3+} should involve in those
348 cases a modest hydrogen deficiency.

349 Looking at the crystal chemical formulae of HU_02 and ST4_11 (Table 6) and taking
350 into consideration the chemical relationships along the alnaperbøeite-(Ce)–perbøeite-(Ce)
351 join (Fig. 3), it is evident that all the heterovalent substitutions leading to a decrease of
352 positive charge at the A sites, i.e. Na for Ca, or Na for REE or Ca for REE, involve a
353 decrement of the mean electron number at the A sites. Indeed, it ranges from 191.3 e^- in
354 HU_02 to 182.5 e^- in ST4_11 (Table 10). It is not possible, however, to determine with
355 certainty at which site Na is incorporated. Taking into account the crystal with the highest Na
356 content (ST4_11, 0.20 Na apfu), ordering of Na at one specific REE site (A2, A3 or A4)
357 would involve a mean electron number < 49 approximately, and can therefore be excluded on
358 the basis of the mean electron number of these sites (Fig. 5). The monotonous decrease of the
359 mean electron number observed as a function of the alnaperbøeitic component for A2, A3,
360 and A4 but not for A1 (Fig. 5, Table 10) could be interpreted as due to Na incorporation at
361 the A2, A3 and A4 sites, with Ca substituted by small, constant amounts of REE at A1 (22.2
362 e^-). On the other hand, all Na could be ordered at A1, if a simultaneous entry of variable
363 amounts of REE (approximately 0.10 apfu in ST4_11) masked the effect of Na on the site
364 scattering. In this case, the replacement of Ca by an increasing (Na+REE) amount in A1
365 along the join alnaperbøeite-(Ce)–perbøeite-(Ce) would account for the decreasing site
366 scattering at A2, A3 and A4.

367 The Si1 and Si2 tetrahedra, linked together to form a Si_2O_7 group, as well as the Si3
368 tetrahedron, are quite similar to the corresponding tetrahedra in epidotes (Franz and Liebscher
369 2004 and references therein); likewise, the Si4 and Si5 tetrahedra can be compared to the
370 homologue ones in törnebohmite-(Ce). We can therefore reasonably assume that no

substitution of Si by other cations occurs at these sites, as also implied by the mean number of 5.00(5) Si apfu for the 54 EMP analyses of the series.

As expected on the basis of the close structural relationship with gatelite-(Ce) (Bonazzi et al. 2003) and västmanlandite-(Ce) (Holtstam et al. 2005), the two O-O contacts suitable for H-bonding (not polyhedral edges) are O11-O4 (2.939-2.990 Å) within the *E* module and O10-O15 (2.642-2.689 Å) within the *T* module, with O11 and O10 as donor oxygens.

STRUCTURE AFTER HEAT TREATMENTS

All geometrical and structural variations induced by heating the crystal of perbøeite-(Ce) in air indicate the development of an oxidation-dehydrogenation process, quite similar to that observed in allanite-group minerals (Bonazzi and Menchetti 1994; Bonazzi et al. 2009). As made evident by the shortening of the mean <M3-O> distance, the divalent iron ordered at the M3 octahedron oxidizes and the charge balance is maintained by concomitant H loss according to the reaction: $^{M3}[Fe^{2+}] + {}^{O10,O11}[OH^-] \rightarrow {}^{M3}[Fe^{3+}] + {}^{O10,O11}[O^{2-}] + \frac{1}{2}H_2$. After the annealing at 450 °C the <M3-O> distance approaches the values corresponding to those due to a site population of Fe^{3+}-Al alone (dotted line in Figure 6) thus indicating that the process is almost complete at that temperature. As the divalent iron decreases, the M3 octahedron becomes more regular [λ values, calculated according to Robinson et al. (1971), decreasing from 1.037 to 1.025].

The loss of H compensating the oxidation of Fe^{2+} is indicated by the variation of the donor–acceptor distances (Table 10). In particular O11-O4 increases from 2.954(6) to 3.134(6) Å while O10-O15 increases more gradually, from 2.642(6) to 2.752(7) Å, suggesting loss of hydrogen mainly from the H1 position, i.e. in the *E* module.

The loss of positive charge on the donor oxygens (O11 and O10) due to partial dehydrogenation at H1 and H2 respectively is balanced mainly by a pronounced shortening of the A4-O11 [from 2.605(3) to 2.403(4) Å] and a moderate shortening of A2-O10 [from 2.674(3) to 2.588(4) Å] distances. The oxygen O11 also approaches M2 [M2-O11 decreasing from 1.883(3) to 1.819(3) Å]. On the contrary, the M2-O10 bond distance, the shortest within the M2 octahedron, does not change significantly with heating.

With regard to the acceptor oxygens (O4 and O15), the loss of positive charge on the O4 oxygen is directly compensated by the oxidation of divalent iron at M3, as shown from the trend of the M3-O4 distance, which decreases from 1.973(3) to 1.892(4) Å, and, to a lesser extent, by the shortening of the M1-O4 distance [from 1.844(2) to 1.819(2) Å]; among the bond distances involving O15, which links Si4 and two A3, the longest A3-O15 is the only decreasing one [from 2.942(5) to 2.797(5) Å].

At the beginning of the heating process, the resulting empirical bond-valence sums on O11 and O10 are 1.29 and 1.28 v.u., respectively, while sums on O4 and O15 are 1.60 and 1.54 v.u., in keeping with the expected hydrogen-bonding system in these minerals. As the heating temperature increases, the total bond strength on the oxygen atoms involved in the O11-H1…O4 bond markedly increases, whereas only small variations are observed for O10-H2…O15 (Table 11), indicating severe dehydrogenation only at the H1 position. In particular, by combining the increase of bond strength on donor with that of acceptor oxygen, the estimated amount of hydrogen loss at H1 position is 0.63 apfu, while only 0.06 apfu appear to be lost at H2 position. On the other hand, the total Fe^{3+} in the crystal (estimated on the basis of the octahedral distances) changes from 0.14 apfu in the untreated crystal to 0.76 apfu after the annealing at 750°C. The hydrogen loss compensating for the Fe^{2+} oxidation, therefore, seems to occur mainly within the *E* module, leaving the *T* module substantially unaffected.

With regard to the unit-cell parameters, the behavior is quite similar to that observed in heated REE-bearing epidote-supergroup minerals (Bonazzi and Menchetti, 1994; Bonazzi et al. 2009). The contraction related to $Fe^{2+} \rightarrow Fe^{3+}$ oxidation results in a decrease of the $ab\sin\beta$ parameter, whereas the relaxation of the O11-H1…O4 bond, which is approximately directed along [001], weakens the link between the M2 and the M1+M3 octahedral chains and results in a lengthening of *c* (Figure 7).

COMPARISON WITH RELATED STRUCTURES

Perbøeite-(Ce) derives from gatelite-(Ce) by the homovalent substitution $[^{M3}Fe^{2+} \rightarrow {}^{M3}Mg]$. Alnaperbøeite-(Ce) derives from perbøeite-(Ce) or gatelite-(Ce) by the coupled heterovalent substitutions $0.5[^{A}Na^{+} \rightarrow {}^{A}REE^{3+}]$ and $[^{M3}Al^{3+} \rightarrow {}^{M3}(Fe^{2+}$ or $Mg)]$.

As concerns the unit-cell dimensions, alnaperbøeite-(Ce) and perbøeite-(Ce), as well as västmanlandite-(Ce), differ from gatelite-(Ce) for the lack of doubling of the translation unit along the **a** axis. The doubling of the translation unit along the **a** axis in gatelite-(Ce), where $a_{gat.} \sim 2a_{epi.} \sim [201]_{tör.}$, appears related to a small offset away from the (010) plane at $y = ¼$ and ¾, which is a mirror in the epidote-supergroup minerals; as a consequence, the space group is $P2_1/a$ instead of $P2_1/m$. Such symmetry deviations are indeed very slight, so that the *hkl* reflections with $h = 2n+1$ are relatively weak. In a quite similar way, törnebohmite-(Ce) ($P2_1/c$) slightly deviates from the $P2_1/m$ symmetry and exhibits weak *hkl* reflections with $l = 2n+1$ leading to a doubling of the *c* parameter (Shen and Moore 1982). In practice, the slight puckering of atomic planes present in törnebohmite-(Ce) and absent in epidotes persists when *E* and *T* modules are combined together in the gatelite-(Ce) structure. The larger the offset from the plane, or the higher the number of atoms deviating from the mirror symmetry, the stronger are the superstructure reflections. Indeed, the weak, continuous streaking at **a***/2 observed in västmanlandite-(Ce) (Holtstam et al. 2005) is due to the offset from the (010)

444 mirror plane of two sites (A3 and O15, occupied by REE and oxygen, respectively), whereas
445 in both alnaperbøeite-(Ce) and perbøeite-(Ce) only O15 exhibits an offset from the mirror
446 plane.
447
448 NOMENCLATURE REMARKS
449 In all members of the epidote–törnebohmite polysomatic series known so far the
450 composition of the *E* module differentiates each member. For internal consistency, the same
451 nomenclature rules as for epidote-supergroup minerals (Armbruster et al. 2006) are applied.
452 Accordingly, the polysomes with *E* = dissakisite, dollaseite, allanite or a new Na-bearing REE
453 epidote-composition deserve four different root names. The name perbøeite-(Ce) is in honor
454 of Per Bøe (b. 1937), a Norwegian geologist and Curator at the Tromsø Museum, who
455 initiated the project that led to the discovery of this species; the name alnaperbøeite-(Ce)
456 emphasizes the chemical relationships with perbøeite-(Ce), the dominance of Al in the M3
457 site and the role of Na to charge balance the dominance of a trivalent cation in the M3 site of
458 the REE-epidote module.
459 In practice, the root name perbøeite should apply to any *ET* polysome with the *E*
460 module deserving the root name allanite (key-sites M3 = Fe^{2+} and A1 = Ca). The root name
461 alnaperbøeite should apply to any *ET* polysome composition in which i) trivalent cations are
462 dominant at the key-site M3 and aluminum is dominant among them and ii) the charge
463 balance in A sites is dominantly achieved by substitution of Na for REE (rather than A^{2+} for
464 REE). The writing of 'alnaperbøeite' without hyphen is deliberate: 'al' and 'na' are not
465 intended as prefixes and, as for the epidote nomenclature, no prefix should be added to the
466 root name if M1 = Al. Otherwise a proper prefix referring to homovalent substitution in M1
467 should be added. Thus, the unnamed mineral from the Bergslagen region (Holtstam et al.
468 2007) having M3 = Fe^{2+} and M1 = Fe^{3+} and reported as Fe^{3+}-analogue of västmanlandite-(Ce)

in the list of unnamed minerals (UM2007-35, Smith and Nickel 2007) is actually the Fe^{3+}-analogue of perbøeite-(Ce) and should be named ferriperbøeite-(Ce). The same name should be assigned to the mineral from eastern Siberia, Russia, described by Gurzhiy et al. (2010), which also exhibits an *E* module of ferriallanite-(Ce) composition.

A THERMODYNAMIC PUZZLE

An intriguing point is the occurrence at the three localities of the constituting *E* and *T* compounds also as single-phase crystals, along with the polysomatic *ET* phase. The absence of reaction textures among them raises the question of the stability of the ordered 1:1 polysome with respect to a mechanical mixture of *E* + *T*, whereby one would expect on thermodynamic grounds the occurrence of either *ET* + *E* or *ET* + *T*, depending on bulk chemistry (as commonly observed in the Bergslagen area for västmanlandite + dollaseite, Holtstam et al. 2005, and 'ferriperbøeite' + ferriallanite, Holtstam and Andersson 2007; but unlike Trimouns where gatelite occurs along with dissakisite and törnebohmite, Bonazzi et al. 2003). The complex texture observed in some perbøeite crystals (Fig. 2) is reminiscent of an exsolution texture, but allanite has not been confirmed in it. The question is of very general bearing, namely that of the stability of any polysome with respect to the mechanical mixture of the end members. The very same question is raised, for instance, by the coexistence of clinochlore with talc in the presence of kulkeite, the ordered 1:1 chlorite–talc mixed-layer (Schreyer et al. 1982), or the occurrence of paragonite with cookeite versus that of their ordered 1:1 mixed-layer, saliotite (Goffé et al. 1994).

IMPLICATIONS: A SODIAN EPIDOTE END-MEMBER

Solid solution towards the new alnaperbøeite-(Ce) *ET* polysome end-member $^{A}(REE_{2.5}CaNa_{0.5})^{M}(Al_4)Si_2O_7(SiO_4)_3O(OH)_2$ accounts for most of the compositional variation

494 observed in crystals from Tysfjord granite pegmatites, as described above. Its very existence
495 raises the question of the role of sodium in the *ET* polysome, in the *E* module and thus in
496 epidote minerals in general, those of the allanite group in particular. Indeed, törnebohmite-
497 (Ce) coexisting with alnaperbøeite-(Ce) is Na-free whereas coexisting allanite-(Ce) is Na-
498 bearing and shows the same charge-compensating coupled substitutions between A and M
499 sites as identified in alnaperbøeite-(Ce) ($Na_{0.5}Al \leftrightarrow REE_{0.5}Fe^{2+}$), although to a much lesser
500 extent (10 mol%). It is therefore extremely tempting to assign Na incorporation to the *E*
501 module alone, *i.e.* into the A1 or A2 sites, leading to the sodian *E* end-member
502 $^{A}(CaREE_{0.5}Na_{0.5})^{M}(Al_3)Si_2O_7(SiO_4)O(OH)$. As shown above, crystallographic evidence is
503 inconclusive as to Na site assignment, site scattering data allowing complete order of Na in
504 A1, or disorder over A2, A3 and A4, or any combination thereof. In the latter two cases, both
505 the *E* and *T* modules would be sodian and no longer be electrically neutral.

506 In any event, if one turns to the epidote-supergroup minerals, sodium is repeatedly
507 reported as a very minor constituent (e.g. Franz and Liebscher 2004) that may become
508 noteworthy only in REE-rich phases, essentially in the allanite group (survey by Gieré and
509 Sorensen 2004). The extreme Na_2O values of 3.28 wt% (Coulson 1997), 1.38 wt% (Semenov
510 et al. 1978) and 0.5 wt% (Bea 1996) reported in allanite can be discarded as due to
511 contamination because the analyses cannot yield a plausible epidote formula. However,
512 values between 0.2 and 0.3 wt% as found here are not uncommon in irrefragable allanite
513 analyses (e.g. Bea 1996, for allanites in granitoid rocks). What is their meaning? The 0.14 to
514 0.21 wt% Na_2O reported in dissakisite from UHP rocks (Yang and Enami 2003) may charge-
515 balance the Ti contents (0.54 to 0.62 wt% TiO_2), through the coupled substitution
516 $^{A}Na^{M}Ti \leftrightarrow {}^{A}Ca^{M}Al$ as suggested by the authors, but as well ThO_2 contents (1.73 to 2.10 wt%) through
517 the coupled substitution $NaTh \leftrightarrow 2REE$ in the A sites. However, alternative substitutions are
518 possible and requested in the absence of Ti or Th, like $^{A}Na^{M}Fe^{3+} \leftrightarrow {}^{A}Ca^{M}Fe^{2+}$ (Yang and

519 Enami 2003) or $^{A}Na^{M}Al \leftrightarrow {}^{A}Ca^{M}Fe^{2+}$ or $^{A}(NaREE) \leftrightarrow {}^{A}(2Ca)$ (Gieré and Sorensen 2004).
520 Actually, the combination of the latter two substitutions, i.e. $Na_{0.5}Al \leftrightarrow REE_{0.5}Fe^{2+}$, is the one
521 that relates perbøeite-(Ce) to alnaperbøeite-(Ce) and which, in allanites, leads to the sodian
522 end-member identified above as a tentative *E* module, namely
523 $(CaREE_{0.5}Na_{0.5})Al_3Si_2O_7(SiO_4)O(OH)$. This new epidote end-member is obviously needed to
524 account for the composition of allanite-group minerals (for up to ca. 10 mol%). This end-
525 member is also needed to account for the chemistry of the *E* module of the new *ET* solid-
526 solution series, even if it is still uncertain whether this electrically neutral formula reflects the
527 actual partitioning of Na among the A sites of the *ET* phase. Clearly, the presence of sodium
528 has to be carefully checked for a complete chemical characterization of the epidote-
529 supergroup and gatelite-group minerals.
530

531 ## ACKNOWLEDGMENTS

532 We thank members of the IMA-CNMNC for demanding and perceptive comments, as
533 well as A. Liebscher and M. Nagashima for accurate reviews. This work was funded by
534 MIUR (project PRIN 2009, "Struttura, microstruttura e proprietà dei minerali") and by the
535 CNRS-INSU Programme DyETI. X-ray intensity data were collected at CRIST, Centro
536 Interdipartimentale di Cristallografia Strutturale, University of Florence, Italy.
537

538 ## REFERENCES CITED

539 Andresen, A. and Tull, J.F. (1986) Age and tectonic setting of the Tysfjord gneiss granite,
540 Efjord, North Norway. Norsk Geologisk Tidsskrift, 66, 69-80.
541 Armbruster, T., Bonazzi, P., Akasaka, M., Bermanec, V., Chopin, C., Gieré, R., Heuss-
542 Assbichler, S., Liebscher, A., Menchetti, S., Pan, Y. and Pasero, M. (2006)

543 Recommended nomenclature of epidote-group minerals. European Journal of
544 Mineralogy, 18, 551-567.
545 Bea, F. (1996) Residence of REE, Y, Th and U in granites and crustal protoliths; implications
546 for the chemistry of crustal melts. Journal of Petrology, 37, 521-552.
547 Bonazzi, P., Bindi, L. and Parodi, G. (2003) Gatelite-(Ce), a new REE-bearing mineral from
548 Trimouns, French Pyrenees: crystal structure and polysomatic relationships with epidote
549 and törnebohmite-(Ce). American Mineralogist, 88, 223-228.
550 Bonazzi, P., Holtstam, D., Bindi, L., Nysten, P. and Capitani, G.C. (2009) Multi-analytical
551 approach to solve the puzzle of an allanite-subgroup mineral from Kesebol, Västra
552 Götaland, Sweden. American Mineralogist, 94, 121-134.
553 Bonazzi, P. and Menchetti, S. (1994) Structural variations induced by heat treatment in
554 allanite and REE-bearing piemontite. American Mineralogist, 79, 1176-1184.
555 Bonazzi, P. and Menchetti, S. (1995) Monoclinic members of the epidote group: effects of the
556 Al $\leftrightarrow$ Fe^{3+} $\leftrightarrow$ Fe^{2+} substitution and of the entry of REE^{3+}. Mineralogy and Petrology,
557 53, 133-153.
558 Brese, N.E. and O'Keeffe, M. (1991) Bond-valence parameters for solids. Acta
559 Crystallographica, B47, 192-197.
560 Coulson, I.M. (1997) Post-magmatic alteration in eudyalite from the North Qoroq center,
561 South Greenland. Mineralogical Magazine, 61, 99-109.
562 Franz, G. and Liebscher, A. (2004) Physical and chemical properties of the epidote minerals -
563 An introduction. Reviews in Mineralogy and Geochemistry, 56, 1-82.
564 Gieré, R. and Sorensen, S.S. (2004) Allanite and other REE-rich epidote-group minerals.
565 Reviews in Mineralogy and Geochemistry, 56, 431-493.

566 Goffé, B., Baronnet, A. and Morin, G. (1994) Saliotite, a new high-pressure, low-temperature
567 metamorphic phyllosilicate mineral: ordered 1:1 cookeite/paragonite mixed-layer.
568 European Journal of Mineralogy, 6, 897-911 [in French].
569 Grew, E.S., Essene, E.J., Peacor, D.R., Su, S.C. and Asami, M. (1991) Dissakisite-(Ce), a new
570 member of the epidote group and the Mg analogue of allanite-(Ce), from Antarctica.
571 American Mineralogist, 76, 1990-1997.
572 Gurzhiy,V. V., Karimova, O.V., Kartashov, P.M. and Krivovichev, S.V. (2010) Crystal
573 structure of a new member of the polysomatic series törnebohmite-epidote from
574 carbonatites of Eastern Siberia. International Mineralogical Association Meeting
575 Budapest, August 2010, Abstract Volume, page 744.
576 Holtstam, D. and Andersson, U.B. (2007) The REE minerals of the Bastnäs-type deposits,
577 South-Central Sweden. Canadian Mineralogist, 45, 1073-1114.
578 Holtstam, D., Kolitsch, U. and Andersson, U.B. (2005) Västmanlandite-(Ce) – a new
579 lanthanide- and F-bearing sorosilicate mineral from Västmanland, Sweden: description,
580 crystal structure, and relation to gatelite-(Ce). European Journal of Mineralogy, 17, 129-
581 141.
582 Husdal, T.A. (2008) The minerals of the pegmatites within the Tysfjord granite, northern
583 Norway. Kongsberg Mineralsymposium 2008, 5-28.
584 Kartashov, P., Ferraris, G., Ivaldi, G., Sokolova, E., and McCammon, C.A. (2002)
585 Ferriallanite-(Ce), $CaCeFe^{3+}AlFe^{2+}(SiO_4)(Si_2O_7)O(OH)$, a new member of the epidote
586 group: description, X-ray and Mössbauer study. Canadian Mineralogist, 40, 1641-1648.
587 Kolitsch, U., Mills, S. J., Miyawaki, R., and Blass, G. (2012) Ferriallanite-(La), a new
588 member of the epidote supergroup from the Eifel, Germany. European Journal of
589 Mineralogy, 24, 741-747.

590 Malcherek, T., Mihailova, B., Schlüter, J. and Husdal, T.A. (2012) Atelisite-(Y), a new rare
591 earth defect silicate of the KDP structure type. European Journal of Mineralogy, 24,
592 1053-1060.
593 Mandarino, J.A. (1976) The Gladstone-Dale relationship-part I: derivation of new constants.
594 Canadian Mineralogist, 14, 498-502.
595 Mills, S. J., Hatert, F., Nickel, E.H. and Ferraris, G. (2009) The standardisation of mineral
596 group hierarchies: application to recent nomenclature proposals. European Journal of
597 Mineralogy, 21, 1073-1080.
598 Oxford Diffraction (2006) *CrysAlis* RED (Version 1.171.31.2) and ABSPACK in *CrysAlis*
599 RED. Oxford Diffraction Ltd, Abingdon, Oxfordshire, England.
600 Peacor, D.R. and Dunn, P.J. (1988) Dollaseite-(Ce) (magnesium orthite redefined): structure
601 refinement and implications for F + M^{2+} substitutions in epidote-group minerals.
602 American Mineralogist, 73, 838-842.
603 Pekov, I.V., Zubkova, N.V., Chukanov, N.V., Husdal, T.A., Zadov, A.E. and Pushcharovsky,
604 D.Y. (2011) Fluorbritholite-(Y), $(Y,Ca,Ln)_5[(Si,P)O_4]_3F$, a new mineral of the britholite
605 group. Neues Jahrbuch für Mineralogie, Abhandlungen, 188, 191-197.
606 Pouchou, J.L. and Pichoir, F. (1984) A new model for quantitative X-ray microanalysis. La
607 Recherche aérospatiale, 3, 167-192 [in French].
608 Raade, G., Johnsen, O., Erambert, M. and Petersen, O.V. (2007) Hundholmenite-(Y) from
609 Norway – a new mineral species in the vicanite group: descriptive data and crystal
610 structure. Mineralogical Magazine, 71, 179-192.
611 Robinson, K., Gibbs, G.V., and Ribbe, P.H. (1971) Quadratic elongation: a quantitative
612 measure of distortion in coordination polyhedra. Science, 172, 567-570.
613 Rouse, R.C. and Peacor, D.R. (1993) The crystal structure of dissakisite-(Ce), the Mg
614 analogue of allanite-(Ce). Canadian Mineralogist, 31, 153-157.

615 Schlüter, J., Malcherek, T. and Husdal, T.A. (2009) The new mineral stetindite, $CeSiO_4$, a
616 cerium end-member of the zircon group. Neues Jahrbuch für Mineralogie,
617 Abhandlungen, 186, 195-200.
618 Schreyer, W., Medenbach, O., Abraham, K., Gebert, W. and Müller, W.F. (1982) Kulkeite, a
619 new metamorphic phyllosilicate mineral: ordered 1:1 chlorite/talc mixed-layer.
620 Contributions to Mineralogy and Petrology, 80, 103-109.
621 Semenov, E.J., Upendran R. and Subramanian, V. (1978) Rare earth minerals of the
622 carbonatites of Tamil Nadu. Journal of the geological Society of India, 19, 550-557.
623 Sheldrick, G.M. (2008) A short history of SHELX. Acta Crystallographica, A64, 112-122.
624 Shen, J. and Moore, P.B. (1982) Törnebohmite, $RE_2Al(OH)[SiO_4]_2$: crystal structure and
625 genealogy of RE(III)Si(IV)↔Ca(II)P(V) isomorphisms. American Mineralogist, 67,
626 1021-1028.
627 Smith, D.G.W. and Nickel, E.H. (2007) A system of codification for unnamed minerals:
628 report of the Subcommittee for Unnamed Minerals of the IMA Commission on New
629 Minerals, Nomenclature and Classification. Canadian Mineralogist, **45**, 983-1055.
630 Wilson, A. J. C. and Prince, E., Eds. (1999) *International Tables for X-ray Crystallography*,
631 Volume C: Mathematical, physical and chemical tables (2nd Edition), Kluwer
632 Academic, Dordrecht, NL.
633 Yang, J.J. and Enami, M. (2003) Chromian dissakisite-(Ce) in a garnet lherzolite from the
634 Chinese Su-Lu UHP metamorphic terrane: Implications for Cr incorporation in epidote-
635 group minerals and recycling of REE into the Earth's mantle. American Mineralogist,
636 88, 604-610.

637

638 CAPTIONS OF FIGURES

639

FIGURE 1. Schematic representation of the structure ([010] projection) of gatelite-group minerals in terms of *E*-type and *T*-type modules.

FIGURE 2. Backscattered-electron image of perbøeite-(Ce) (medium gray) - törnebohmite-(Ce) (light gray) intergrowths within a matrix of yttrian fluorite (dark gray). Sample ST4, Stetind.

FIGURE 3. Chemical variations along the perbøeite-(Ce)–alnaperbøeite-(Ce) join. Element contents are given in atoms per formula unit (on the basis of Si+P+Al+Ti+Fe+Mg = 9): REE includes Y and Th; Ca includes Ba and Mn; Fe includes Mg. Empty symbols refer to chemical data reported in Table 7; black symbols represent perbøeite-(Ce) and alnaperbøeite-(Ce) single crystals (Table 6).

FIGURE 4. Unit-cell content in perbøeite-(Ce) - alnaperbøeite-(Ce).

FIGURE 5. Variation of the mean electron number derived from the refined site scattering in each A site vs. their sum in the untreated crystals of the perbøeite-(Ce) and alnaperbøeite-(Ce) series. The monotonous decrease observed for A2, A3, and A4 as a function of the alnaperbøeitic component can be due to Na incorporation at A2, A3 and A4 sites with constant A1 population, or to Ca incorporation at A2, A3 and A4 with complete ordering into A1 of Na with enough REE to maintain site scattering (see text).

FIGURE 6. Variation of the <M3-O> octahedral distance as a function of the Fe content obtained by site-scattering refinement. Dotted line ($y = 1.968 + 0.087x$) refers to natural (Al, Fe^{3+})-epidotes and dashed line ($y = 1.968 + 0.207x$) is calculated for an (Al, Fe^{2+}) site population (<Fe^{2+}- O> = 2.175 Å) (Bonazzi and Menchetti 1995). Black squares refer to the untreated crystals wherein Fe is present mainly as Fe^{2+}; black circles refer to the perbøeite-(Ce) crystal (ST2_02) heated in air at increasing temperatures. After the heating at 450 °C in air the <M3-O> distance approaches the values corresponding to those due to a site population of Fe^{3+}-Al alone.

FIGURE 7. The $ab\sin\beta$ value plotted against the c unit-cell parameter for ST2_02 crystal heated in air (black circles) and for the untreated crystals (black squares). As the heating temperature increases, the $Fe^{2+} \rightarrow Fe^{3+}$ oxidation causes a contraction of the M3-M1 octrahedral chain mainly resulting in a decrease of the $ab\sin\beta$ parameter; the relaxation of the O11-H1…O4 bond due to the hydrogen loss weakens the link between the M2 and the M1+M3 octahedral chains and results in a lengthening of c. In the absence of complete chemical characterization including Fe^{2+}/Fe^{3+} ratio or H determination, it is not easy to establish whether the spread of values observed for the untreated crystals is only due to the variation of the alnaperbøeite-(Ce) component or whether a modest hydrogen deficiency also occurs.

TABLE 1 – Experimental details for the selected crystals

	ST4_11	**ST4_09**	**ST3_01**	**NE_01**	**ST4_10**	**ST4_02**	**ST2_01**	**ST2_03**	**HU_02**
a (Å)	8.9277(6)	8.9310(5)	8.9205(4)	8.9546(8)	8.9222(4)	8.9165(4)	8.9327(4)	8.9313(9)	8.9110(4)
b (Å)	5.6548(6)	5.6574(3)	5.6573(3)	5.6675(5)	5.6650(2)	5.6754(2)	5.6817(2)	5.6608(6)	5.6866(2)
c (Å)	17.587(1)	17.6000(9)	17.5715(9)	17.652(2)	17.569(1)	17.5253(7)	17.5807(7)	17.549(2)	17.5252(7)
β (°)	116.475(8)	116.517(4)	116.500(4)	116.677(7)	116.470(5)	116.321(3)	116.465(3)	116.396(8)	116.300(5)
V (Å^3)	794.8(1)	795.71(8)	793.59(7)	800.5(1)	794.92(7)	794.92(6)	798.77(6)	794.8(2)	796.13(7)
data collection									
θ_{max} (°)	35.68	33.30	33.25	34.23	34.82	28.86	33.79	32.34	34.92
total refl. collected	8111	6562	6816	7140	7589	3598	7953	6861	7576
unique refl. (R_{int})	3705 (4.01)	3040 (4.43)	3030 (4.29)	3313 (7.00)	3417 (4.02)	1968 (2.46)	3209 (3.84)	2829 (4.48)	3460 (3.57)
refl. with $F > 4\sigma(F)$	2637	1942	1995	1546	2224	1593	2269	1830	2679
structure refinement									
number of parameters	202	206	206	206	206	206	206	206	206
R_1 [$F > 4\sigma(F)$]	5.19	4.57	4.28	5.08	3.94	2.76	3.60	3.77	4.14
R_1 all	8.19	8.15	7.25	12.41	7.34	3.79	6.05	7.04	6.12
Max ΔF peak (e$^-$/Å^3)	3.06	2.23	2.87	2.50	2.61	0.98	2.50	2.14	2.09
Min ΔF peak (e$^-$/Å^3)	-2.17	-1.66	-2.84	-1.28	-1.72	-0.90	-1.74	-1.77	-2.50

	ST2_04	**HU_01**	**ST2_02**	**ST2_02-350**	**ST2_02-450**	**ST2_02-550**	**ST2_02-650**	**ST2_02-750**
a (Å)	8.8996(4)	8.8950(4)	8.9039(3)	8.9044(3)	8.9002(3)	8.9031(3)	8.8979(4)	8.8936(4)
b (Å)	5.6759(4)	5.6827(2)	5.6785(2)	5.6650(2)	5.6304(2)	5.6290(1)	5.6235(2)	5.6189(2)
c (Å)	17.5154(9)	17.5044(7)	17.5039(6)	17.5261(7)	17.7324(6)	17.7392(6)	17.731(1)	17.7550(7)
β (°)	116.221(4)	116.240(3)	116.301(4)	116.399(5)	116.710(3)	116.752(4)	116.815(5)	116.952(5)
V (Å^3)	793.71(8)	793.63(6)	793.39(5)	791.88(6)	793.78(5)	793.85(5)	791.81(7)	790.89(7)
data collection								
θ_{max} (°)	35.00	34.88	32.53	34.67	33.01	34.96	34.95	34.87
total refl. collected	7621	7722	8188	7535	6736	7926	7630	7709
unique refl. (R_{int} %)	3432 (4.23)	3475 (7.44)	2848 (3.07)	3413 (2.79)	3043 (2.87)	3424 (2.57)	3431 (3.84)	3449 (3.29)
refl. with $F > 4\sigma(F)$	2405	1712	2280	2739	2433	2722	2643	2718
structure refinement								
number of parameters	206	203	206	206	203	203	203	203

R_1 [$F > 4\sigma(F)$] (%)	4.57	4.47	2.97	3.62	3.04	3.05	3.48	3.47
R_1 all (%)	7.21	11.47	4.22	4.94	4.16	4.26	5.06	4.87
Max ΔF peak ($e^-/Å^3$)	4.54	1.95	1.66	2.27	1.57	2.71	2.28	2.85
Min ΔF peak ($e^-/Å^3$)	-2.62	-1.62	-2.03	-3.04	-2.71	-3.43	-3.15	-4.31

Note: crystals labeled ST, NE, and HU come from Stetind, Nedre Eivollen and Hundholmen pegmatites, respectively. The ST_02 crystal was annealed for 48 h at 350, 450, 550, 650 and 750 °C.

TABLE 2 – Refined site occupancy, fractional atomic coordinates and equivalent isotropic displacement parameters (Å^2) for alnaperbøeite-(Ce) (ST4_11 crystal) and perbøeite-(Ce) (HU_02 crystal).

atom	occupancy	*x*	*y*	*z*	U_{iso}
A1	$Ca_{0.942(4)}Ce_{0.056}$	0.7322(2)	¼	0.4097(1)	0.0229(5)
	$Ca_{0.958(2)}Ce_{0.042}$	0.7322(2)		0.40998(8)	0.0182(4)
A2	$Ce_{0.896(6)}Ca_{0.104}$	0.88965(6)	¼	0.24991(3)	0.0198(2)
	$Ce_{0.978(4)}Ca_{0.022}$	0.89185(5)		0.24954(2)	0.0154(1)
A3	$Ce_{0.888(6)}Ca_{0.112}$	0.73978(8)	¼	0.01013(4)	0.0375(2)
	$Ce_{0.958(4)}Ca_{0.042}$	0.73949(6)		0.00968(3)	0.0311(2)
A4	$Ce_{0.858(6)}Ca_{0.142}$	0.08128(6)	¾	0.16453(3)	0.0198(2)
	$Ce_{0.950(4)}Ca_{0.050}$	0.07839(5)		0.16574(2)	0.0148(1)
M1	$Al_{1.000}$	½	½	½	0.0137(4)
	$Al_{0.992(7)}Fe_{0.008}$				0.0112(6)
M2	$Al_{0.973(8)}Fe_{0.027}$	0.4827(1)	- 0.0005(3)	0.2051(1)	0.0132(5)
	$Al_{0.973(6)}Fe_{0.027}$	0.4813(1)	0.0005(2)	0.20530(8)	0.0113(4)
M3	$Al_{0.598(9)}Fe_{0.402}$	0.1988(2)	¾	0.3756(1)	0.0207(6)
	$Fe_{0.716(7)}Al_{0.284}$	0.1950(1)		0.37640(7)	0.0139(3)
Si1		0.1627(2)	¼	0.4755(1)	0.0135(4)
		0.1625(2)		0.4774(1)	0.0107(3)
Si2		0.8084(2)	¾	0.3374(1)	0.0128(4)
		0.8055(2)		0.3357(1)	0.0104(3)
Si3		0.3072(2)	¼	0.3136(1)	0.0122(4)
		0.3050(2)		0.3126(1)	0.0095(3)
Si4		0.6723(2)	¾	0.1043(2)	0.0160(4)
		0.6697(2)		0.1030(1)	0.0118(4)
Si5		0.1564(2)	¼	0.0773(1)	0.0119(4)
		0.1553(2)		0.0776(1)	0.0092(3)
O1		0.2668(5)	0.4926(7)	0.4783(3)	0.0224(9)
		0.2674(4)	0.4901(5)	0.4824(2)	0.0165(7)
O2		0.1837(5)	0.4802(7)	0.2924(3)	0.0217(8)
		0.1793(4)	0.4750(5)	0.2897(2)	0.0163(7)
O3		0.6982(5)	0.9864(6)	0.2969(3)	0.0189(8)
		0.6943(4)	- 0.0130(5)	0.2980(2)	0.0148(7)
O4		0.4413(6)	¾	0.4240(4)	0.016(1)
		0.4421(5)		0.4248(3)	0.0124(9)
O5		0.4525(7)	¼	0.4140(3)	0.015(1)
		0.4496(5)		0.4129(3)	0.0133(9)

O6		0.4193(6) 0.4188(5)	¼	0.2603(4) 0.2601(3)	0.015(1) 0.0126(9)
O7		- 0.0172(7) - 0.0166(5)	¼	0.3969(4) 0.3967(3)	0.022(1) 0.0152(9)
O8		- 0.0311(9) - 0.0435(7)	¾	0.3207(6) 0.3114(4)	0.038(2) 0.029(1)
O9		0.8654(9) 0.8723(6)	¾	0.4391(4) 0.4386(3)	0.034(2) 0.023(1)
O10		0.5579(6) 0.5581(5)	¼	0.1632(4) 0.1624(3)	0.015(1) 0.0105(8)
O11		0.4065(7) 0.4037(5)	¾	0.2482(4) 0.2484(3)	0.018(1) 0.0117(9)
O12		0.5396(6) 0.5391(5)	¾	0.1471(4) 0.1474(3)	0.014(1) 0.0112(9)
O13		0.2702(5) 0.2685(4)	0.4905(7) 0.4907(5)	0.1104(3) 0.1104(2)	0.0195(8) 0.0157(7)
O14		0.7958(5) 0.7942(4)	0.5232(7) 0.5243(6)	0.1334(3) 0.1321(2)	0.027(1) 0.0200(8)
O15	$O_{0.50}$ $O_{0.50}$	0.555(1) 0.5496(8)	0.817(1) 0.818(1)	0.0047(5) 0.0033(4)	0.031(2) 0.022(2)
O16		0.063(1) 0.0613(8)	¼	- 0.0232(5) - 0.0229(4)	0.056(2) 0.042(2)
O17		0.0235(9) 0.0233(6)	¼	0.1163(5) 0.1164(4)	0.043(2) 0.029(1)
H1		- 0.434(8)	¾	- 0.325(4)	- 0.01(2)

Note: For each atom, the first row refers to alnaperbøeite-(Ce), the second one to perbøeite-(Ce)

TABLE 5 –X-ray powder diffraction data

(1)		(2)		(3)				
alnaperbøeite-(Ce)		perbøeite-(Ce)						
I_{calc}	d_{calc}	I_{calc}	d_{calc}	I_{obs}	d_{obs}	h	k	l
91.88	15.7426	91.34	15.7111	75	15.7	0	0	1
13.68	7.9914	18.32	7.9886	15	7.98	1	0	0
12.21	7.5326	16.21	7.5051	15	7.49	-1	0	2
6.91	4.7739	6.24	4.7900	-	-	-1	1	1
9.60	4.6639	9.94	4.6628	-	-	1	0	2
29.90	4.6160	33.18	4.6327	30	4.62	1	1	0
8.96	4.5925	7.21	4.6063	-	-	0	1	2
6.65	4.3908	5.88	4.3749	-	-	-1	0	4
7.13	4.1504	7.39	4.1629	-	-	1	1	1
6.17	3.9357	6.67	3.9278	-	-	0	0	4
41.60	3.4986	43.95	3.5014	40	3.489	-2	1	2
17.94	3.4681	17.67	3.4675	15	3.461	-1	1	4
5.87	3.3768	5.30	3.3767	-	-	-2	1	3
12.41	3.2633	13.09	3.2686	10	3.268	2	1	0
18.63	3.0553	17.77	3.0553	15	3.061	2	0	2
100.00	2.9831	100.00	2.9805	100	2.971	-1	1	5
7.86	2.9688	6.40	2.9625	-	-	-3	0	3
7.10	2.8815	6.28	2.8733	-	-	-3	0	4
47.37	2.8274	48.13	2.8433	50	2.828	0	2	0
32.33	2.7509	31.31	2.7503	30	2.739	0	1	5
7.67	2.6881	6.37	2.6914	-	-	2	1	2
17.24	2.6655	18.05	2.6787	15	2.667	1	2	0
22.82	2.6587	23.32	2.6584	20	2.660	2	0	3
10.29	2.6286	9.72	2.6273	-	-	-3	1	3
56.54	2.6188	58.50	2.6190	60	2.619	-3	1	2
5.43	2.4891	5.11	2.4988	-		0	2	3
16.52	2.4488	14.60	2.4447	15	2.442	-3	1	5
6.11	2.2953	7.19	2.2865	-	-	-3	0	7
11.42	2.2612	10.49	2.2662	10	2.262	-2	2	4
14.59	2.1823	15.29	2.1799	15	2.181	-4	0	2
25.80	2.1431	25.46	2.1464	25	2.140	-2	2	5
9.91	2.1037	10.20	2.1083	10	2.101	0	2	5
7.04	2.0812	6.36	2.0828	-	-	3	1	2
18.18	2.0752	16.95	2.0814	15	2.078	2	2	2
5.31	2.0656	5.24	2.0648	-	-	2	0	5
17.26	1.9369	18.37	1.9418	20	1.940	2	2	3
11.11	1.9164	11.26	1.9176	10	1.921	3	1	3
6.81	1.8692	6.26	1.8698	-	-	-2	2	7
12.70	1.8435	11.99	1.8426	10	1.842	1	1	7
6.00	1.7276	6.47	1.7300	-	-	-4	2	2

8.11	1.6945	7.60	1.6899	-	-	-1	0	10
12.41	1.6608	12.52	1.6668	-	-	-1	3	5
7.02	1.6484	6.06	1.6479	-	-	-5	1	2
12.21	1.6332	13.37	1.6325	-	-	-4	2	7
10.31	1.5891	11.00	1.5948	10	1.591	-3	3	2
5.42	1.4916	5.45	1.4902	-		-2	2	10
12.34	1.4137	11.98	1.4217	10	1.419	0	4	0

Notes: in columns (1) and (2) are reported the calculated powder pattern for alnaperbøeite-(Ce) and perbøeite-(Ce), obtained using atomic parameters of the crystals ST4_11 and HU2_02, respectively; (3) experimental powder pattern for the solid solution.

TABLE 6 – Electron-microprobe analyses (mean and range of # point-analyses, in wt %) and atomic ratios on a $O_{20}(OH)_2$ basis for the selected crystals of perbøeite and alnaperbøeite.

	ST4_11	range	HU2_02	range	ST2_02	range
#	15		5		4	
Na_2O	0.56	0.84 – 0.54	0.22	0.21 – 0.23	0.26	0.24 – 0.27
CaO	5.74	5.76 – 5.25	5.00	4.94 – 5.06	5.07	5.11 – 5.04
MnO *	0.18	0.00 – 0.24	0.20	0.16 – 0.24	0.18	0.12 – 0.29
BaO	0.04	0.00 – 0.10	0.04	0.00 – 0.08	0.05	0.02 – 0.09
La_2O_3	6.29	4.87 – 6.41	7.43	7.27 – 5.52	6.67	6.65 – 6.69
Ce_2O_3	17.29	15.63 – 17.40	19.07	18.52 – 19.48	18.35	18.28 – 18.42
Pr_2O_3	2.52	2.33 – 2.68	2.43	2.30 – 2.50	2.38	2.30 – 2.46
Nd_2O_3	9.31	8.40 – 11.74	9.41	9.04 – 10.02	11.25	11.16 – 11.34
Sm_2O_3	2.02	1.91 – 2.29	1.62	1.52 – 1.68	1.97	1.78 – 2.16
Gd_2O_3	1.13	0.83 – 1.34	0.91	0.87 – 0.95	0.78	0.77 – 0.79
Dy_2O_3	0.56	0.09 – 0.57	0.49	0.34 – 0.72	0.13	0.02 – 0.24
Ho_2O_3	0.04	0.00 – 0.18	0.00	0.00 – 0.00	0.13	0.11 – 0.16
Er_2O_3	0.12	0.00 – 0.30	0.18	0.01 – 0.27	0.35	0.27 – 0.44
Yb_2O_3	0.12	0.05 – 0.15	0.03	0.00 – 0.10	0.08	0.00 – 0.16
Y_2O_3	1.29	1.00 – 1.57	0.60	0.56 – 0.65	0.75	0.68 – 0.81
ThO_2	0.37	0.16 – 0.50	0.17	0.14 – 0.22	0.12	0.10 – 0.14
MgO	0.09	0.02 – 0.12	0.01	0.00 – 0.01	0.11	0.10 – 0.13
FeO *	2.67	0.95 – 3.06	5.05	4.87 – 5.25	5.05	5.02 – 5.09
Al_2O_3	16.71	16.48 – 19.08	14.67	14.49 – 14.88	14.29	14.17 – 14.41
SiO_2	27.79	27.50 – 27.83	26.95	26.50 – 27.04	26.98	26.79 – 27.16
total	94.84	94.00 – 95.70	94.48	93.93 – 94.87	94.95	94.79 – 95.19
Na	0.20		0.08		0.09	
Ca	1.10		1.00		1.01	
Mn^{2+}	0.03		0.03		0.03	
Ba	0.00		0.00		0.00	
La	0.42		0.51		0.46	
Ce	1.14		1.30		1.25	
Pr	0.16		0.16		0.16	
Nd	0.60		0.62		0.75	
Sm	0.13		0.10		0.13	
Gd	0.07		0.06		0.05	
Dy	0.03		0.03		0.01	
Ho	0.00		0.00		0.01	
Er	0.01		0.01		0.02	
Yb	0.01		0.00		0.00	
Y	0.12		0.06		0.07	
Th	0.02		0.01		0.01	
ΣREE+Th	2.71		2.86		2.92	
Σ(A cat)	4.04		3.97		4.05	
Mg	0.02		0.00		0.03	
Fe^{2+}	0.40		0.79		0.79	
Al	3.54		3.21		3.13	
Σ(M cat)	3.96		4.00		3.95	
Si	4.99		5.01		5.02	

total	12.98	12.99	13.01

Notes: * Mn and Fe assumed as divalent.

Table 8a. Electron-microprobe analyses of allanite (A) and törnebohmite (T) coexisting with perbøeite/alnaperbøeite in Stetind (ST) and Nedre Eivollen (NE).

	Allanite-(Ce)				Törnebohmite-(Ce)			
Sample	NE	NE	ST2	range	ST2	range	ST4	range
#	1	1	8		5		3	
Na_2O	0.28	0.29	0.12	(0.06 - 0.18)	0.01	(0.00 - 0.02)	0.02	(0.01 - 0.04)
CaO	9.08	9.65	7.61	(6.31 - 8.48)	0.20	(0.17 - 0.25)	0.14	(0.09 - 0.20)
MnO	0.50	0.58	2.58	(0.73 - 4.83)	0.00	(0.00 - 0.00)	0.00	(0.00 - 0.00)
SrO	0.00	0.02	0.01	(0.00 - 0.07)	0.02	(0.00 - 0.09)	0.01	(0.00 - 0.03)
BaO	0.00	0.00	0.02	(0.00 - 0.09)	0.08	(0.02 - 0.14)	0.04	(0.00 - 0.08)
La_2O_3	2.99	2.66	3.24	(2.68 - 3.84)	6.53	(5.55 8.26)	4.57	(2.64 - 6.34)
Ce_2O_3	11.38	10.62	11.63	(11.08 - 12.30)	22.17	(18.26 - 25.61)	18.35	(12.08 - 23.08)
Pr_2O_3	1.88	1.75	1.84	(1.70 - 1.96)	3.84	(3.51 - 4.02)	3.43	(3.28 - 3.63)
Nd_2O_3	7.46	7.96	8.38	(7.25 - 9.20)	19.33	(16.81 - 20.53)	21.03	(17.68 - 26.39)
Sm_2O_3	1.73	1.62	1.51	(1.19 - 1.76)	4.49	(3.12 - 5.72)	6.47	(4.89 - 7.77)
Gd_2O_3	0.65	0.89	0.49	(0.00 - 0.85)	2.22	(1.69 - 3.32)	3.33	(2.59 - 3.88)
Dy_2O_3	0.11	0.00	0.13	(0.00 - 0.33)	0.85	(0.44 - 1.30)	1.56	(1.24 - 1.75)
Ho_2O_3	0.03	0.00	0.05	(0.00 - 0.23)	0.21	(0.00 - 0.44)	0.20	(0.11 - 0.34)
Er_2O_3	0.22	0.09	0.16	(0.00 - 0.36)	0.00	(0.00 - 0.00)	0.43	(0.28 - 0.53)
Yb_2O_3	0.10	0.03	0.05	(0.00 - 0.08)	0.14	(0.00 - 0.22)	0.19	(0.15 - 0.21)
Y_2O_3	0.34	0.34	0.29	(0.17 - 0.38)	1.74	(0.97 - 2.76)	2.14	(2.02 - 2.24)
ThO_2	0.00	0.04	0.04	(0.00 - 0.17)	0.21	(0.00 - 0.56)	0.07	(0.00 - 0.20)
MgO	0.03	0.07	0.15	(0.10 - 0.21)	0.00	(0.00 - 0.02)	0.00	(0.00 - 0.00)
MnO	0.50	0.58	2.58	(0.73 - 4.83)	0.00	(0.00 - 0.00)	0.00	(0.00 - 0.00)
FeO tot.	10.78	9.96	11.90	(11.33 - 12.73)	0.04	(0.00 - 0.08)	0.00	(0.00 - 0.00)
Al_2O_3	18.47	19.16	16.55	(15.01 - 16.86)	9.77	(9.37 - 10.10)	9.87	(9.74 - 10.10)
SiO_2	30.99	31.24	30.35	(29.77 - 30.81)	22.87	(22.02 - 23.54)	23.35	(22.95 - 23.90)
Total	97.02	96.97	97.10	(96.31 - 98.11)	94.72	(92.44 - 96.02)	95.20	(94.85 - 95.51)
Basis	25 charges	25 charges	25 charges		17 charges		17 charges	
Na	0.053	0.054	0.023		0.002		0.003	
Ca	0.945	0.994	0.811		0.019		0.013	
Mn	0.041	0.047	0.217		0.000		0.000	
Sr	0.000	0.001	0.001		0.001		0.001	
Ba	0.000	0.000	0.001		0.003		0.001	
La	0.107	0.094	0.119		0.211		0.146	
Ce	0.404	0.374	0.423		0.711		0.583	

Pr	0.067	0.061	0.067	0.123	0.108
Nd	0.259	0.273	0.298	0.605	0.652
Sm	0.058	0.054	0.052	0.136	0.193
Gd	0.021	0.028	0.016	0.064	0.096
Dy	0.003	0.000	0.004	0.024	0.044
Ho	0.001	0.000	0.002	0.006	0.006
Er	0.007	0.003	0.005	0.000	0.012
Yb	0.003	0.001	0.002	0.004	0.005
Y	0.018	0.017	0.015	0.081	0.099
Th	0.000	0.001	0.001	0.004	0.001
REE + Th	0.948	0.906	1.004	1.969	1.945
Σ(A cat)	1.987	2.002	2.057	1.994	1.963
Mg	0.004	0.010	0.022	0.000	0.000
Fe^{2+}	0.875	0.801	0.989	0.003	0.000
Al	2.113	2.170	1.939	1.009	1.009
Σ(M cat)	2.992	2.981	2.950	1.012	1.009
Si	3.009	3.002	3.017	2.003	2.026
Σcat	7.987	7.986	8.023	5.007	4.998

Note : Ti and P below detection limit. # = number of point analyses.

Table 8b. Electron-microprobe analyses of minerals coexisting with perbøeite/alnaperbøeite in Stetind (ST) and Nedre Eivollen (NE).

	fluorite	fluorite	kuliokite	hundhol.?	F-thalenite	thalenite	F-brithol.
Sample	NE	ST2	ST4	ST2	NE	NE	NE
Na_2O	0.32	0.22	0.01	0.20	0.01	0.00	0.11
CaO	52.53	58.65	0.70	5.43	0.07	0.18	9.89
SrO	0.08	0.00	0.00	0.00	0.03	0.00	0.02
BaO	0.00	0.04	0.06	0.00	0.00	0.03	0.00
La_2O_3	0.64	0.30	0.04	2.74	0.19	0.80	1.32
Ce_2O_3	1.97	0.85	0.11	9.42	1.19	5.12	7.63
Pr_2O_3	0.33	0.13	0.19	1.43	0.42	1.45	1.51
Nd_2O_3	1.42	1.00	2.07	11.31	3.51	8.19	10.40
Sm_2O_3	0.70	0.30	2.12	5.23	3.05	4.43	4.95
Gd_2O_3	0.71	0.39	5.83	5.42	5.42	5.40	5.23
Dy_2O_3	1.08	0.76	6.57	4.01	7.50	6.59	5.87
Ho_2O_3	0.34	0.19	0.91	0.39	0.92	0.93	0.67
Er_2O_3	0.89	0.57	6.03	2.95	7.35	5.76	3.91
Yb_2O_3	1.09	0.57	3.69	1.69	6.63	5.39	2.92
Y_2O_3	14.93	11.09	39.62	18.85	28.53	23.21	16.57
ThO_2	0.00	0.01	0.00	0.02	0.00	0.13	0.20
MgO	0.00	0.00	0.00	0.00	0.00	0.00	0.00
MnO	0.00	0.00	0.00	0.02	0.00	0.00	0.30
FeO tot.	0.00	0.00	0.00	0.41	0.00	0.00	0.25
Al_2O_3	0.00	0.00	6.85	1.33	0.00	0.00	0.00
SiO_2	0.00	0.00	15.53	14.35	28.20	28.19	21.77
F	44.20	46.94	11.76	6.86	3.06	0.10	2.53
– F = O	–18.61	–19.77	–4.95	–2.89	–1.29	–0.04	–1.07
Total	102.62	102.24	97.14	89.17	94.79	95.86	94.98
Basis	1 cation	1 cation	23 charges	Si = 7 pfu	21 charges	21 charges	25 charges
Na	0.009	0.006	0.003	0.189	0.002	0.000	0.029
Ca	0.827	0.886	0.097	2.838	0.008	0.021	1.458
Sr	0.001	0.000	0.000	0.000	0.002	0.000	0.002
Ba	0.000	0.000	0.003	0.000	0.000	0.001	0.000
La	0.003	0.002	0.002	0.493	0.008	0.032	0.067
Ce	0.011	0.004	0.005	1.682	0.047	0.202	0.384
Pr	0.002	0.001	0.009	0.254	0.017	0.057	0.076

Nd	0.007	0.005	0.096	1.970	0.136	0.315	0.511
Sm	0.004	0.001	0.094	0.879	0.114	0.165	0.235
Gd	0.003	0.002	0.250	0.876	0.195	0.193	0.239
Dy	0.005	0.003	0.273	0.630	0.262	0.229	0.260
Ho	0.002	0.001	0.037	0.061	0.032	0.032	0.029
Er	0.004	0.003	0.245	0.452	0.250	0.195	0.169
Yb	0.005	0.002	0.145	0.251	0.219	0.177	0.123
Y	0.117	0.083	2.724	4.893	1.644	1.332	1.213
Th	0.000	0.000	0.000	0.002	0.000	0.003	0.006
REE + Th	0.163	0.107	3.881	12.445	2.921	2.932	3.312
Mg	0.000	0.000	0.000	0.000	0.000	0.000	0.000
Mn	0.000	0.000	0.000	0.008	0.000	0.000	0.035
Fe^{2+}	0.000	0.000	0.000	0.167	0.000	0.000	0.029
Al	0.000	0.000	1.043	0.765	0.000	0.000	0.000
Si	0.000	0.000	2.007	7.000	3.053	3.039	2.995
F	2.055	2.094	4.805	10.583	1.048	0.034	1.101
ΣCat	1.000	1.000	7.033	23.413	5.987	5.993	7.860

Note : Ti and P below detection limit, also for fluor-britholite-(Y).

TABLE 9 – Physical and optical properties of alnaperbøeite-(Ce) and perbøeite-(Ce)

	alnaperbøeite-(Ce)	perbøeite-(Ce)
morphology	prismatic, elongated along [010]	prismatic, elongated along [010]
color	grayish very pale green	grayish green
streak	white	white
lustre	vitreous, transparent	vitreous, transparent
hardness (Mohs)	6-7	6-7
tenacity	brittle	brittle
cleavage	{100} good, {001} imperfect	{100} good, {001} imperfect
parting	none observed	none observed
fracture	irregular	irregular
calculated density (g/cm^3)*	4.308	4.474
mean refractive index*	1.757	1.775
n_x	1.778(2) colorless	1.788(2) colorless
n_y	1.784(2) colorless	1.793(2) grayish blue
n_z	1.810(5) colorless	1.820(5) colorless
$2V_z$	33.5(5)°	30.0(5)°
optical plane	(010)	(010)
Z $\wedge$(001) [?]	30(3)°	17(1)°
dispersion	inclined (slightly stronger)	inclined (very weak)

*calculated with the chemical analyses given in Table 6. The mean refractive index was obtained according to the Gladstone-Dale relationship (Mandarino 1976).

TABLE 10 – Selected structural parameters for the investigated crystals

	ST4_11	ST4_09	ST3_01	NE_01	ST4_10	ST4_02	ST2_01	ST2_03	HU_02
$<A1\text{-}O>^{VII}$	2.487	2.488	2.481	2.487	2.481	2.477	2.480	2.474	2.470
n. e^-	22.2	22.0	22.0	23.1	22.4	21.1	22.1	22.1	21.6
$<A2\text{-}O>^{VIII}$	2.570	2.573	2.571	2.584	2.574	2.575	2.580	2.579	2.575
n. e^-	54.0	55.0	55.2	54.6	55.8	56.8	56.1	56.4	57.2
$<A3\text{-}O>^{VIII}$	2.598	2.603	2.601	2.610	2.597	2.596	2.603	2.598	2.595
n. e^-	53.7	54.7	55.0	55.0	55.7	56.2	55.6	55.9	56.4
$<A4\text{-}O>^{X}$	2.653	2.650	2.646	2.658	2.623	2.652	2.656	2.652	2.676
n. e^-	52.6	53.7	53.7	53.3	54.4	55.9	55.3	55.4	56.1
<M1-O>	1.923	1.928	1.924	1.930	1.925	1.928	1.928	1.926	1.931
n. e^-	13.0	13.3	13.1	13.4	13.3	13.1	13.3	13.4	13.1
<M2-O>	1.895	1.894	1.893	1.898	1.895	1.897	1.897	1.897	1.899
n. e^-	13.4	13.6	13.4	13.7	13.3	13.2	13.5	13.5	13.4
<M3-O>	2.051	2.051	2.062	2.061	2.067	2.085	2.094	2.098	2.107
n. e^-	18.2	18.9	18.9	19.2	19.8	20.7	21.1	21.6	22.4
$^{M3}(Fe^{3+})_{calc}$	0.00	0.08	0.00	0.05	0.07	0.04	0.02	0.06	0.08
<Si1-O>	1.626	1.622	1.618	1.620	1.619	1.626	1.621	1.618	1.625
<Si2-O>	1.615	1.615	1.619	1.623	1.616	1.618	1.619	1.616	1.617
<Si3-O>	1.646	1.648	1.648	1.647	1.645	1.641	1.647	1.637	1.639
<Si4-O>	1.634	1.638	1.635	1.639	1.630	1.631	1.635	1.628	1.637
<Si5-O>	1.620	1.621	1.623	1.615	1.615	1.620	1.620	1.617	1.617
O11-O4	2.967(10)	2.975(9)	2.974(9)	2.99(1)	2.968(7)	2.945(7)	2.975(7)	2.965(8)	2.956(7)
O10-O15	2.689(10)	2.68(1)	2.66(1)	2.66(1)	2.661(7)	2.665(8)	2.686(7)	2.665(8)	2.653(8)

	ST2_04	HU_01	ST2_02	ST2_03-350	ST2_02-450	ST2_02-550	ST2_02-650	ST2_02-750
$<A1\text{-}O>^{VII}$	2.466	2.469	2.471	2.472	2.481	2.484	2.481	2.483
n. e^-	22.2	21.4	21.1	21.1	21.5	21.1	21.1	20.8
$<A2\text{-}O>^{VIII}$	2.581	2.581	2.575	2.571	2.562	2.558	2.553	2.550

n. e^-	57.0	57.0	55.8	56.9	56.9	56.9	56.5	56.9
$<A3\text{-}O>^{VIII}$	2.599	2.594	2.594	2.593	2.588	2.588	2.581	2.578
n. e^-	55.9	56.2	56.1	56.1	56.1	56.1	56.5	56.9
$<A4\text{-}O>^{X}$	2.647	2.650	2.649	2.645	2.646	2.645	2.641	2.637
n. e^-	55.9	55.9	55.8	55.7	55.7	55.7	56.1	56.1
<M1-O>	1.925	1.928	1.926	1.924	1.916	1.917	1.917	1.916
n. e^-	13.0	13.7	13.1	13.3	13.4	13.4	13.5	13.6
<M2-O>	1.892	1.898	1.893	1.893	1.896	1.897	1.898	1.897
n. e^-	13.4	13.4	13.4	13.3	13.5	13.4	13.3	13.5
<M3-O>	2.099	2.103	2.102	2.079	2.029	2.029	2.026	2.025
n. e^-	22.5	22.6	22.0	21.8	21.6	21.7	21.8	21.3
$^{M3}(Fe^{3+})_{calc}$	0.17	0.15	0.07	0.25	0.63	0.65	0.69	0.63
<Si1-O>	1.616	1.621	1.623	1.622	1.627	1.626	1.628	1.623
<Si2-O>	1.618	1.618	1.615	1.619	1.619	1.619	1.616	1.617
<Si3-O>	1.646	1.638	1.641	1.641	1.646	1.648	1.645	1.646
<Si4-O>	1.634	1.627	1.638	1.630	1.628	1.634	1.627	1.629
<Si5-O>	1.618	1.614	1.620	1.619	1.614	1.612	1.609	1.611
O11-O4	2.949(9)	2.939(9)	2.954(6)	2.972(7)	3.094(1)	3.113(6)	3.121(6)	3.134(6)
O10-O15	2.661(9)	2.672(9)	2.642(6)	2.670(7)	2.717(7)	2.728(6)	2.746(7)	2.752(7)

Note: distances are given in (Å); n. e^- = mean electron number obtained from occupancy refinement. Standard deviations for the individual metal-oxygen distances are in the 0.001 – 0.009 (Å) range; the highest values regard the distances involving the O15 atom.

TABLE 11 – Bond-strengths (*v.u.*) on the four oxygen atoms involved in the hydrogen bonding system in the untreated ST2_02 crystal before and after the heating in air at 750° C.

ST2_02	A2	A3	A4	M1	M2	M3	Si4	
	$Ce^{3+}_{0.97}Ca_{0.03}$	$Ce^{3+}_{0.95}Ca_{0.05}$	$Ce^{3+}_{0.94}Ca_{0.06}$	$Al_{0.99}Fe^{3+}_{0.01}$	$Al_{0.97}Fe^{3+}_{0.03}$	$Fe^{2+}_{0.62}Al_{0.31}Fe^{3+}_{0.07}$	$Si_{1.00}$	
O11			0.293		0.497^{x2}			**1.29**
O4				0.557^{x2}		0.483		**1.60**
O10	0.248				0.515^{x2}			**1.28**
O15		0.119+0.362					1.056	**1.54**
ST2_02-750	A2	A3	A4	M1	M2	M3	Si4	
	$Ce_{0.97}Ca_{0.03}$	$Ce_{0.97}Ca_{0.03}$	$Ce_{0.95}Ca_{0.05}$	$Al_{0.95}Fe^{3+}_{0.05}$	$Al_{0.96}Fe^{3+}_{0.04}$	$Fe^{3+}_{0.63}Al_{0.36}Fe^{2+}_{0.01}$	$Si_{1.00}$	
O11			0.506		0.595^{x2}			**1.70**
O4				0.598^{x2}		0.619		**1.82**
O10	0.311				0.507^{x2}			**1.32**
O15		0.176+0.363					1.016	**1.56**

Note: calculated from the bond-valence curves of Brese and O'Keeffe (1991).

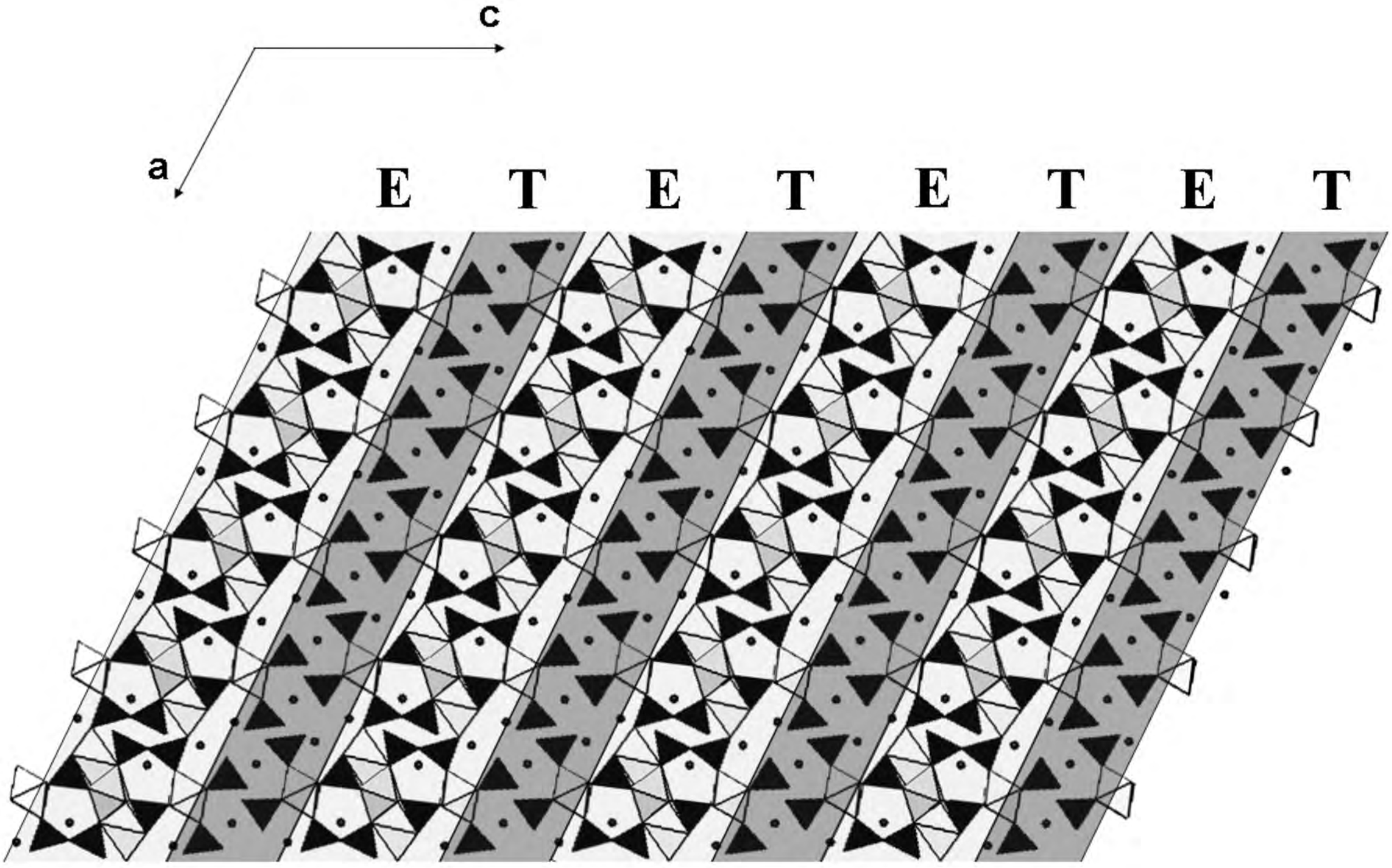
c
a
E T E T E T E T

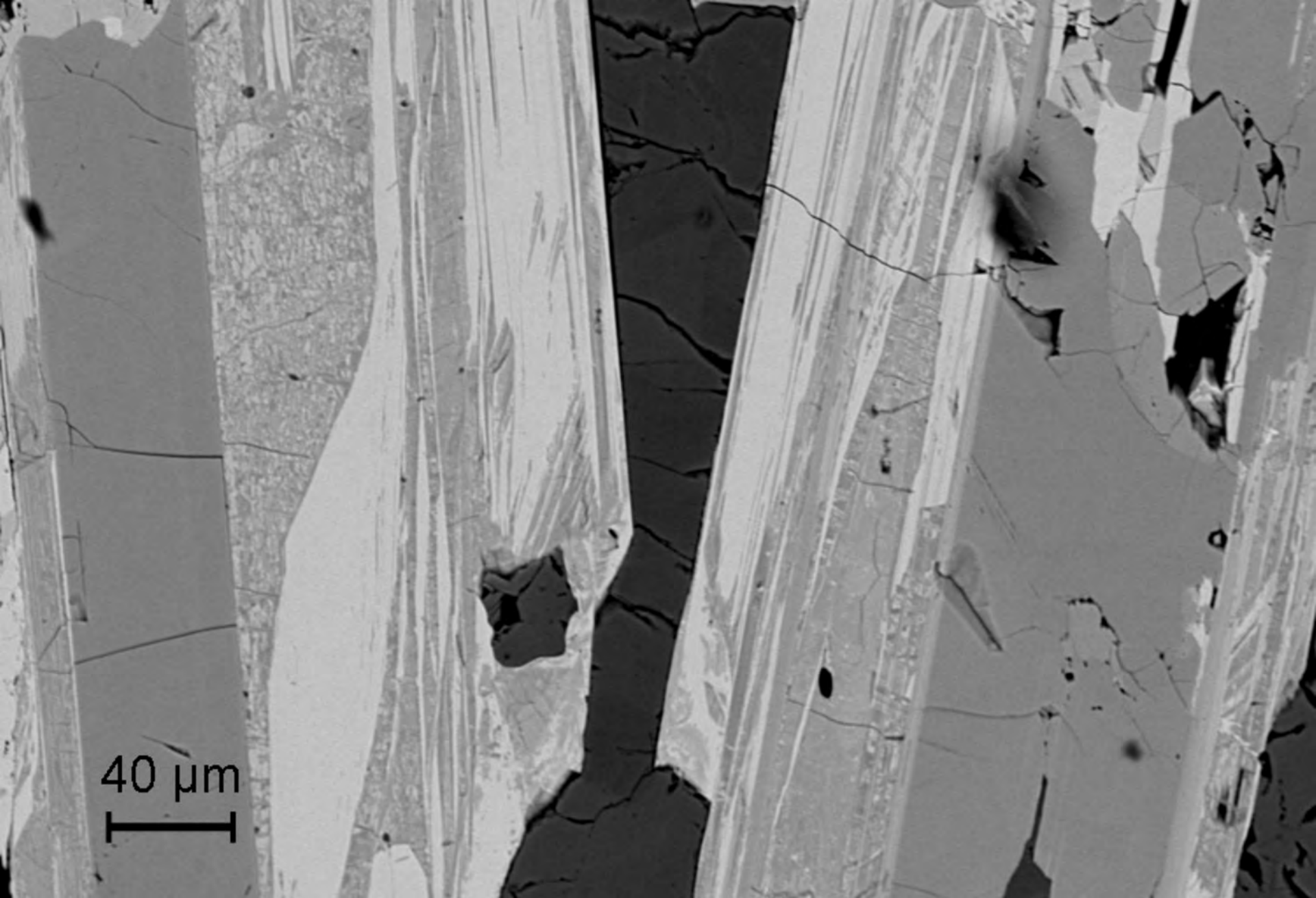
40 µm

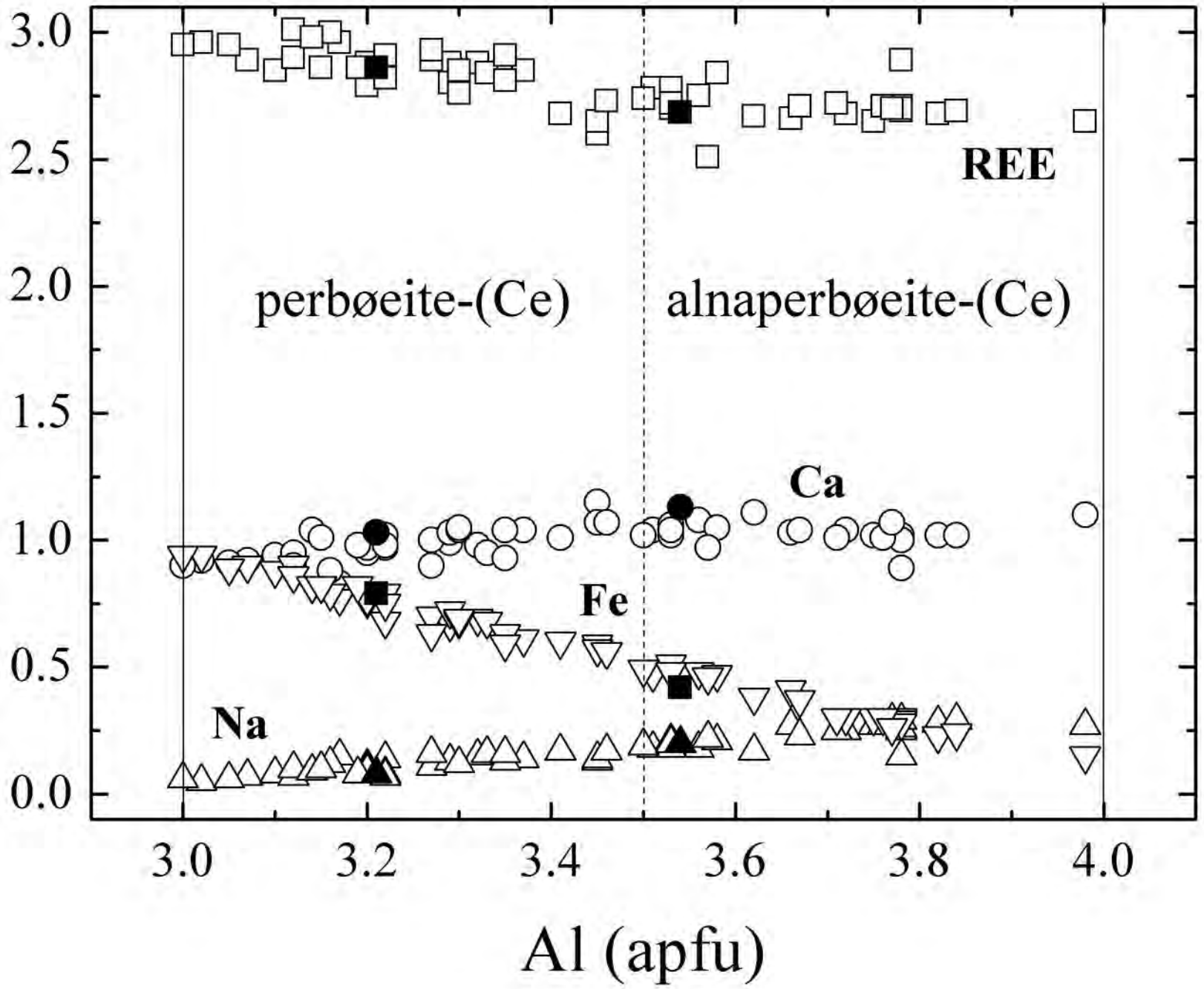
3.0
2.5
2.0
1.5
1.0
0.5
0.0
REE
perbøeite-(Ce)
alnaperbøeite-(Ce)
Ca
Fe
Na
3.0
3.2
3.4
3.6
3.8
4.0
Al (apfu)

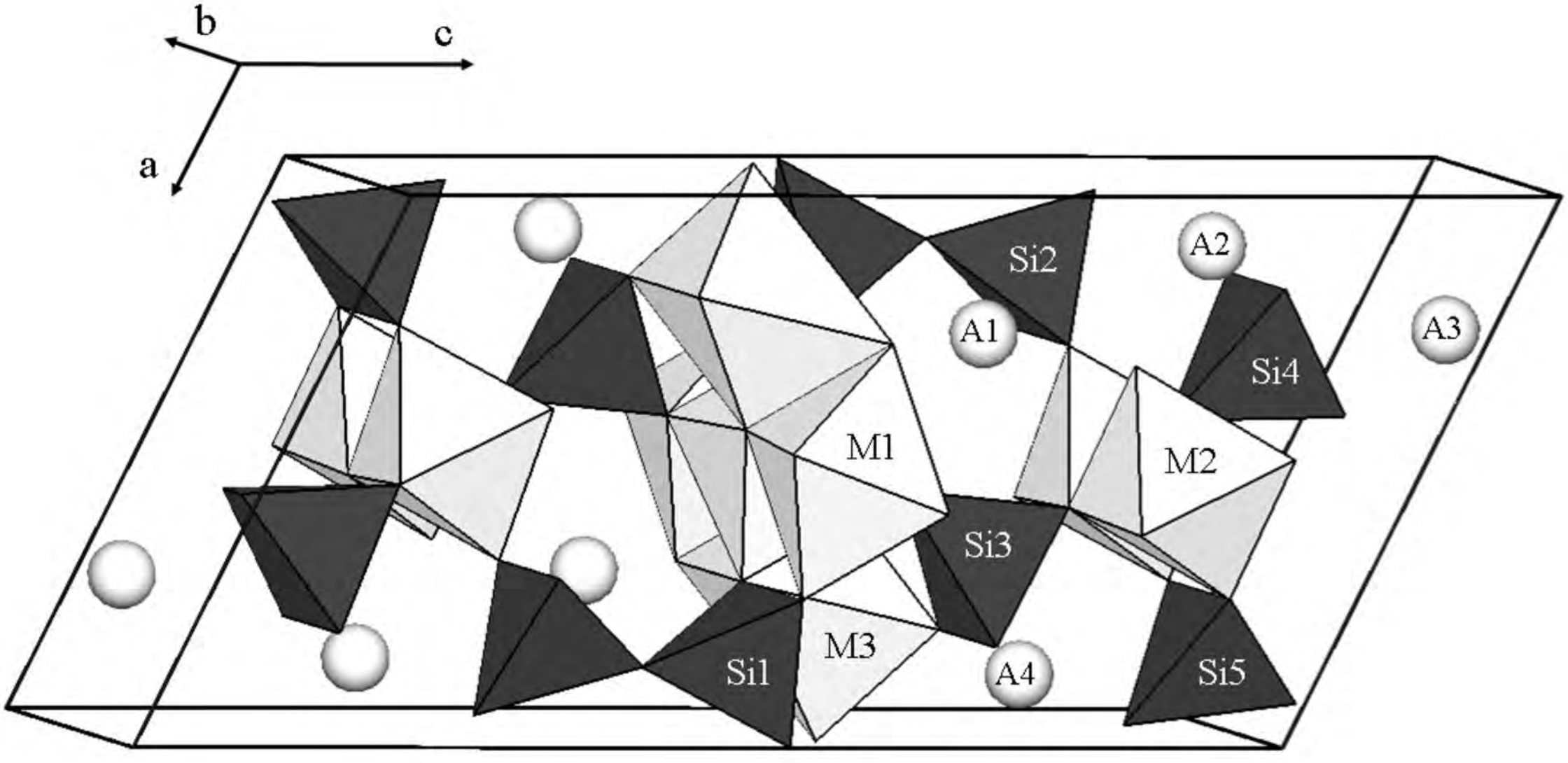
b
c
a
Si2
A2
A1
A3
Si4
M1
M2
Si3
M3
Si1
A4
Si5

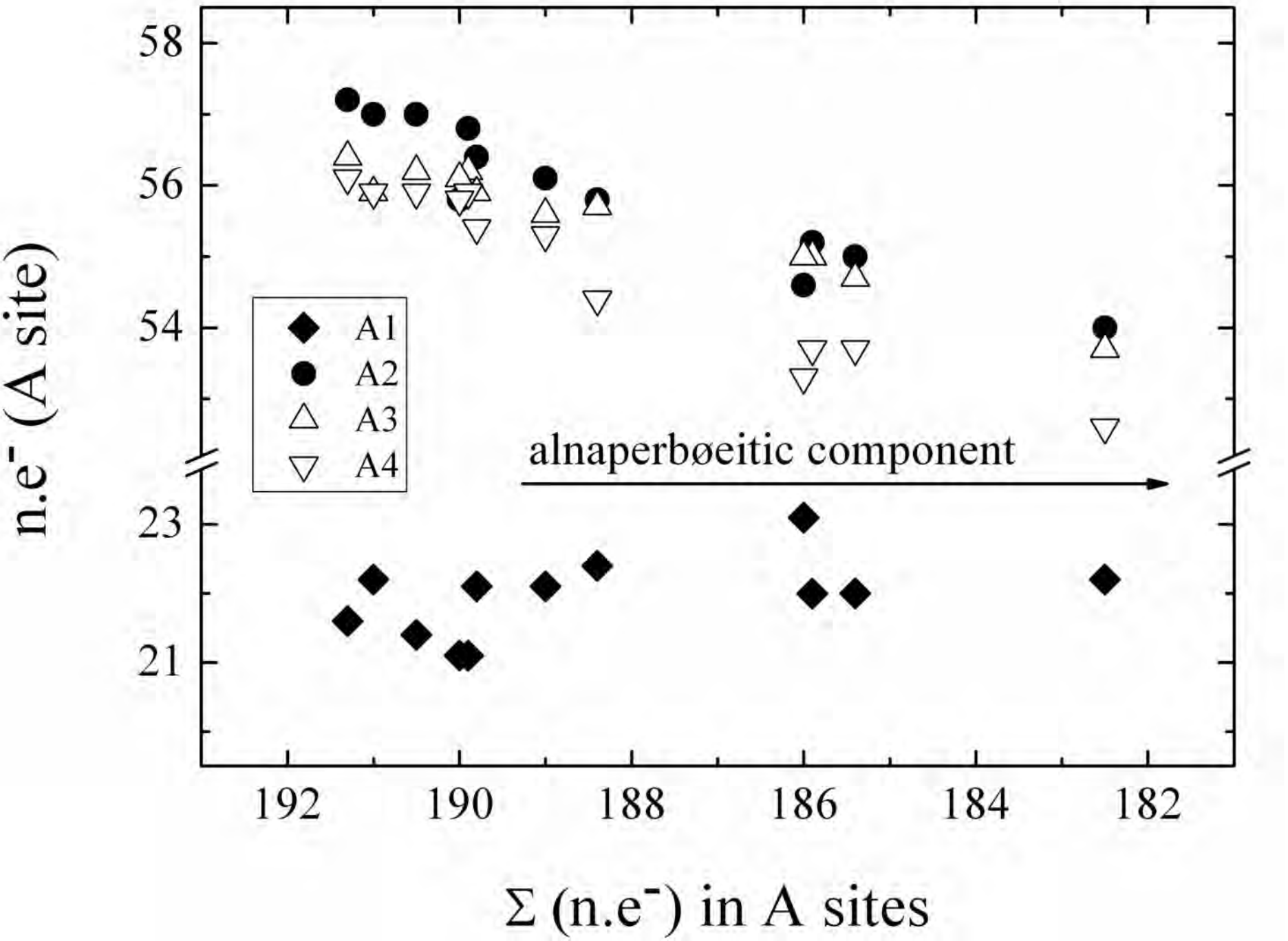
58
56
54
23
21
n.e⁻ (A site)
A1
A2
A3
A4
alnaperbøeitic component
192
190
188
186
184
182
Σ (n.e⁻) in A sites

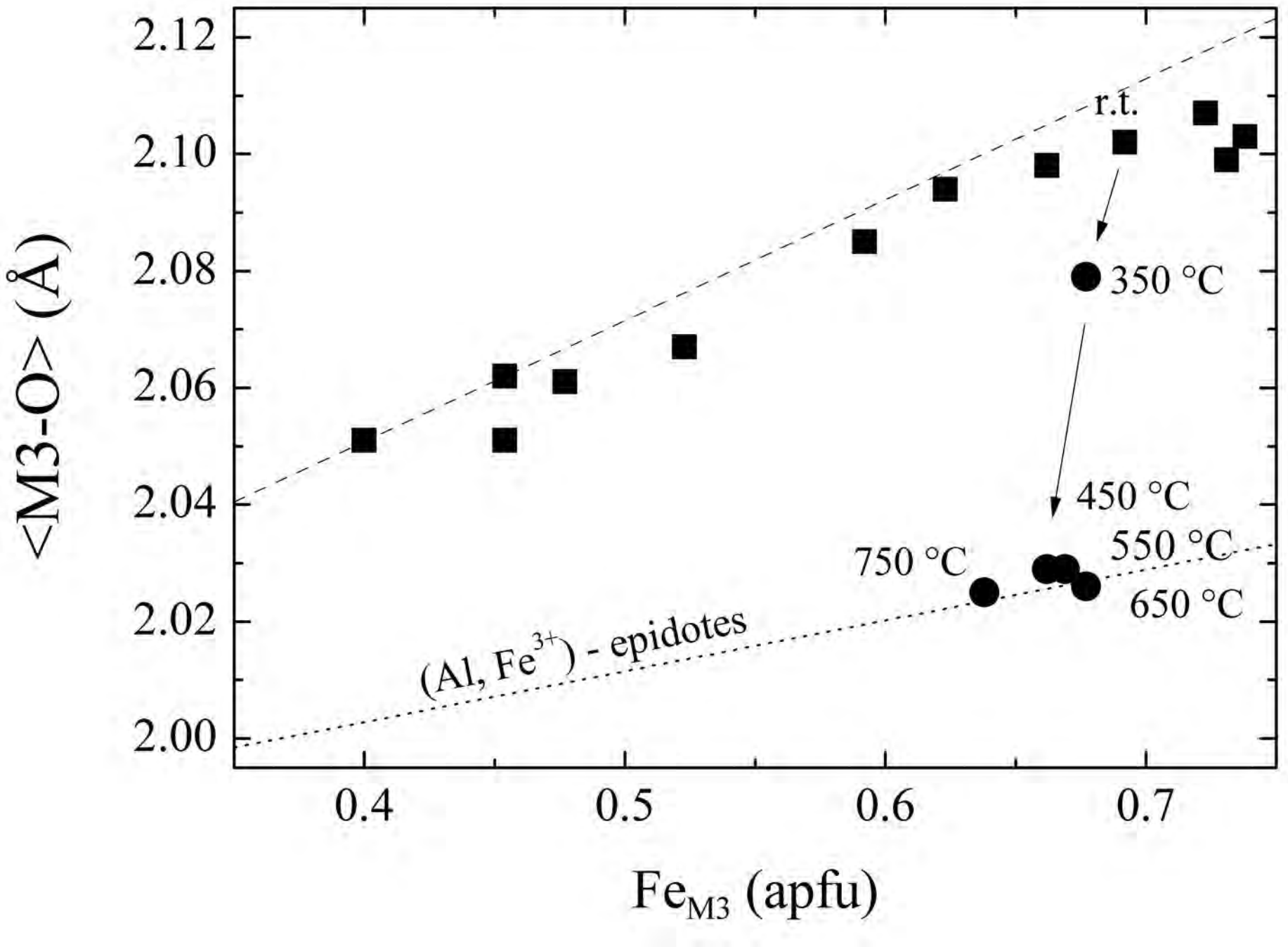
2.12
2.10
2.08
2.06
2.04
2.02
2.00
<M3-O> (Å)
0.4
0.5
0.6
0.7
Fe$_{M3}$ (apfu)
r.t.
350 °C
450 °C
550 °C
650 °C
750 °C
(Al, Fe^{3+}) - epidotes

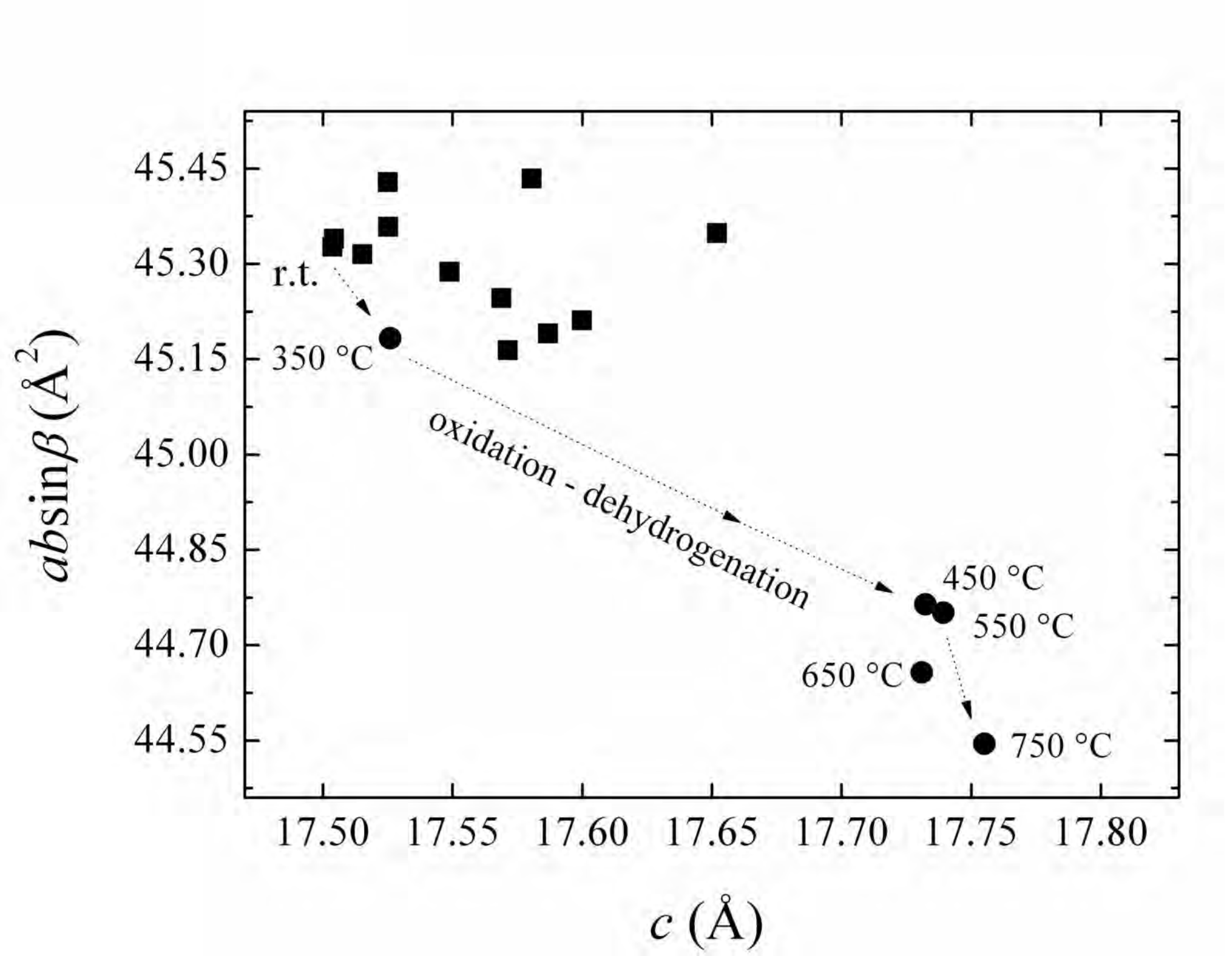
45.45
45.30
45.15
45.00
44.85
44.70
44.55
17.50
17.55
17.60
17.65
17.70
17.75
17.80
$ab\sin\beta$ (Å^2)
c (Å)
r.t.
350 °C
oxidation - dehydrogenation
450 °C
550 °C
650 °C
750 °C